NACA

RESEARCH MEMORANDUM

STATIC TESTS OF A SHROUDED AND AN UNSHROUDED PROPELLER
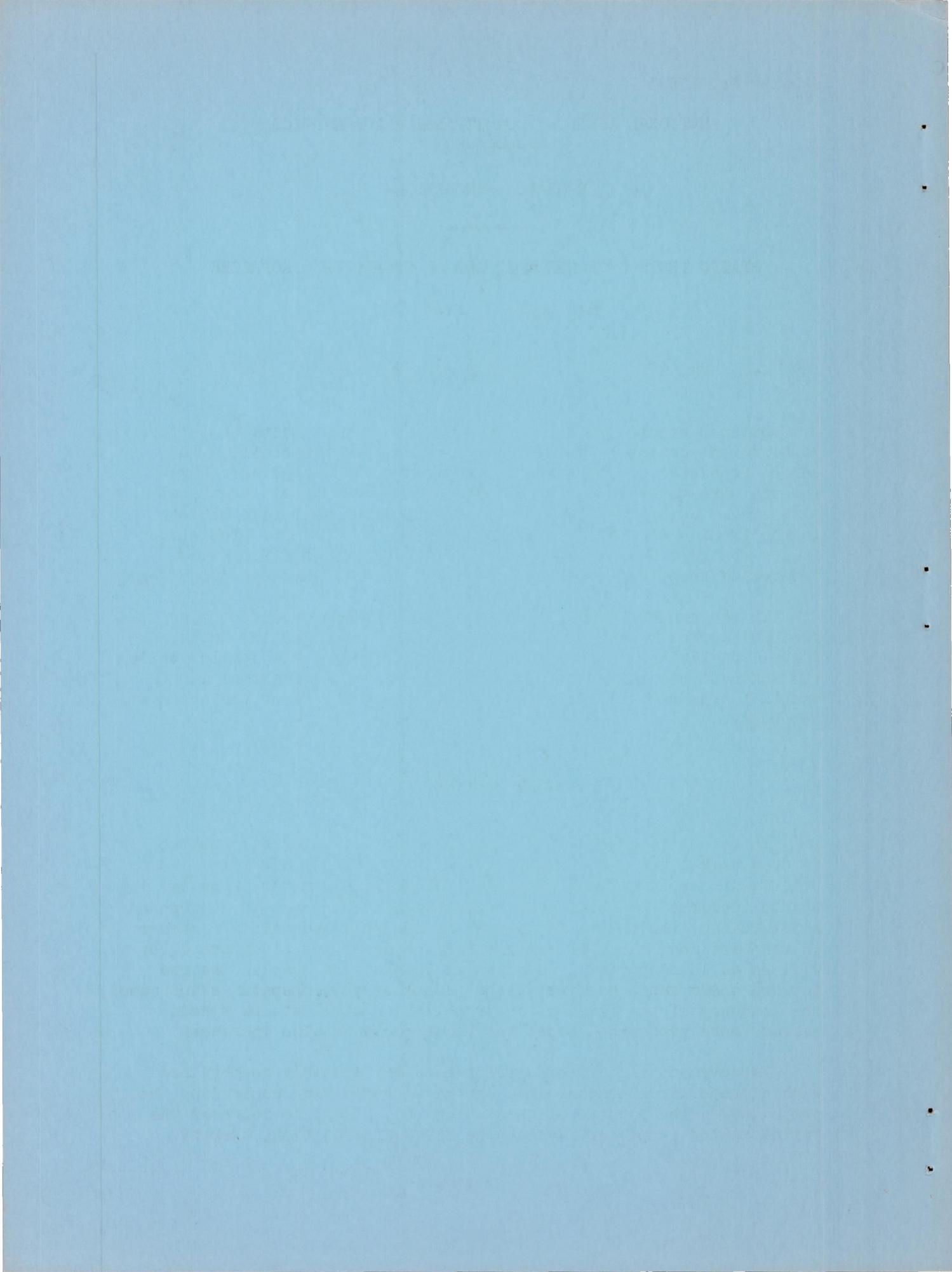
By

Robert J. Platt, Jr.

Langley Memorial Aeronautical Laboratory
Langley Field, Va.

NATIONAL ADVISORY COMMITTEE
FOR AERONAUTICS
WASHINGTON

February 9, 1948

NATIONAL ADVISORY COMMITTEE FOR AERONAUTICS

RESEARCH MEMORANDUM

STATIC TESTS OF A SHROUDED AND AN UNSHROUDED PROPELLER

By Robert J. Platt, Jr.

SUMMARY

Outdoor static tests were made on two high-solidity propellers of different design, one shrouded and the other unshrouded. The shroud consisted of a fixed ring encircling the propeller. Three shrouds were tested to determine the effects of shroud length and exit area. Both propellers were dual-rotating, with five blades in the front component and seven in the rear component. The blade angles tested ranged from 15° to 40° in 5° increments for the unshrouded propeller and from 35° to 45° for the shrouded propeller.

In the range tested, for equal power the shrouded propeller produced approximately twice as much static thrust as the unshrouded propeller chiefly because the unshrouded propeller was stalled while the shrouded propeller was unstalled. Variations of shroud length and exit area had little effect on the static thrust of the shrouded propeller.

INTRODUCTION

In recent years the controllable-pitch propeller has come to be used on all but the smallest of propeller-driven aircraft. For some future applications, however, a controllable-pitch propeller may not be feasible for mechanical reasons, as in the case of a proposed gas turbine. The use of a fixed-pitch propeller entails a decrease in take-off and climb performance because the fixed-pitch propeller will be at least partially stalled at low forward speeds. As the forward speed range over which the propeller must operate is increased, the tendency of the fixed-pitch propeller to stall at low speeds becomes more pronounced since the blade angle is also increased.

Improvement in take-off performance may possibly be obtained with a propeller operating in a shroud (a fixed ring encircling the propeller). The purpose of this shroud is, first, to increase the inflow at the propeller disc at the take-off condition, thereby

decreasing the angle of attack of the blade-section elements to an angle at which the blades are no longer stalled and, second, to increase the cross-sectional area of the slipstream.

The present report presents static test data for two high-solidity, dual-rotating propellers of different design, one shrouded and the other unshrouded. The tests were made over a range of blade angles and tip Mach numbers. In the case of the shrouded propeller, three shrouds of different lengths and ratios of shroud exit area to area at the propeller plane were tested. The thrust on the shrouds was measured as well as the thrust and torque acting on each component of the dual-rotating propellers.

Further information on shrouded propellers may be obtained from a German report (reference 1) which includes both static and wind-tunnel tests. Static tests of shrouded propellers with three and four blades are given in reference 2.

SYMBOLS

The symbols used are as follows:

M_t propeller tip Mach number

R propeller tip radius, feet

r station radius, feet

x radial station (r/R)

β blade angle measured at $0.75R$, degrees

S cross-sectional area of jet, square feet

V velocity of jet, feet per second

m mass flow, slugs per second

p static pressure, pounds per square foot

ρ air density, slugs per cubic foot

D propeller diameter, feet

N propeller rotational speed, revolutions per minute

n   propeller rotational speed, revolutions per second

T   thrust, pounds

P   power absorbed by propeller, foot-pounds per second

C_T thrust coefficient $\left(\dfrac{T}{\rho n^2 D^4}\right)$

C_P power coefficient $\left(\dfrac{P}{\rho n^3 D^5}\right)$

C_p shroud pressure coefficient $\left(\dfrac{p - p_o}{\rho n_F^2 D^2}\right)$

l length of shroud, feet

θ diffuser expansion angle

Subscripts:

F   front propeller component

R   rear propeller component

S   shroud

o   station far ahead of propeller

2   station directly behind propeller

3   station at exit of shroud

4   station far behind propeller

APPARATUS

The dynamometer was located outdoors for these tests. Figures 1 and 2 show the test setup with the unshrouded and shrouded propellers. Figure 3 shows a diagram of the dynamometer with the shrouded propeller. The model shrouded propeller tested was 48 inches in diameter and the unshrouded propeller was 49 inches in diameter. Both propellers were dual-rotating with five blades in the front component and seven blades in the rear component. The dynamometer was fitted with a cylindrical metal fairing to increase the body diameter to 16 inches at the propeller plane.

Dynamometer.- The dynamometer consisted of two separate driving units, one for each component of the dual-rotating propeller, suspended from a supporting framework by streamlined struts. Within the fixed outer casing of each unit were two directly coupled 200-horsepower induction motors. The outer housings of these motors were mounted in large ball bearings to permit rotation of the housings under torque. These bearings ran on tracks to permit longitudinal movement of the motors under thrust. The motors of each unit were connected by two vertical arms extending through the support struts to a cantilever thrust spring and a torque spring located at the top of each support strut. The dynamometer motors were restrained by these springs. The deflections of the springs due to thrust and torque loads were transmitted by selsyn motors to the nearby control house.

Shrouds.- The first step in the design of the shrouds was to make an analysis of the shrouded propeller performance to determine what ideal efficiency could be obtained from a propeller-shroud combination at the design condition. This analysis was based on the simple momentum theory, which assumes that the flow is incompressible and frictionless. The further assumption is made that the static pressure of the air leaving the shroud exit has reached free-stream pressure. Equating the total pressure just behind the propeller to that at the shroud exit,

$$\frac{1}{2}\rho V_o^2 + p_o + \frac{P}{S_2 V_2} = \frac{1}{2}\rho V_3^2 + p_3$$

$$V_3^2 = V_o^2 + \frac{2P}{\rho S_2 V_2}$$

$$V_3 = \sqrt{V_o^2 + \frac{2P}{m}}$$

From the simple momentum theory, the ideal efficiency,

$$n = \frac{2V_o}{V_o + V_3}$$

The ideal efficiency was computed, by means of the above equations, at several values of the shroud area ratio S_3/S_2 for the following full-scale design condition:

Velocity, miles per hour 250
Horsepower 3440
Rotational speed, revolutions per minute 1800
Propeller diameter, feet 8
Altitude . . . . Sea level

The results of this analysis are shown in figure 4. The figure also shows the effect of the shroud area ratio on the axial velocity at the propeller plane and on the tip Mach number of the propeller. Increasing the ratio of shroud exit area to area at the propeller plane results in an increase in ideal efficiency because the exit velocity is lowered. However, the axial velocity through the propeller is at the same time increased, which results in a higher propeller tip Mach number. An area ratio of 1.1 was arbitrarily chosen for the first shroud as a compromise between the factors of ideal efficiency and compressibility losses. This area ratio permitted the use of a reasonably short shroud length with an expansion angle θ of 7° to insure a good diffuser efficiency. The shroud nose section was obtained by selecting an arbitrary mean line and laying out the ordinates for an ellipse along perpendiculars to this mean line. This original nose was modified at the start of the test to minimize separation of the flow from the shroud nose by increasing the radius of curvature of the inner surface of the nose. This shroud was termed the short cruise shroud.

Two additional shrouds were designed with the area ratio S_3/S_2 increased to a value of 1.3. The first of these, the short take-off shroud, was identical with the short cruise shroud except for the greater area ratio and greater diffuser angle. It simulated the cruise shroud with flaps open for take-off, the diffuser expansion angle being 22.4°. The second take-off shroud was of longer diffuser length to decrease the expansion angle to a value of 14.4°. Ordinates for the longitudinal sections of the shrouds with the modified nose are given in table I and the sections are shown in figure 5.

The shrouds were rigidly constructed of wood and steel and were fixed to the dynamometer casing by four streamline struts. In addition, wire bracing parallel to the propeller plane proved necessary to prevent serious vibration of the shroud. For the purpose of determining the shroud thrust, each shroud was fitted with 37 static-pressure orifices distributed along the chord over the inner and outer surfaces at the bottom of the shroud. The pressure leads were led out through a tube at the top of the shroud to the rear dynamometer support strut and thence to a multiple-tube manometer located in the control house. For an independent check of the shroud thrust, electrical strain gages were fastened to the shroud support strut fittings at the points of attachment to the dynamometer casing.

Propellers.- The shrouded propeller was designed to operate
with the cruise shroud at the design condition. The method used
was similar to that for ducted fans (reference 3). In designing
the propeller, it was assumed that the axial-velocity distribution
at the propeller plane was uniform. Blade-form curves for this
propeller are shown in figure 6.

The unshrouded propeller was made up of blades which originally
were designed as a two-blade propeller to provide minimum induced
losses with a blade angle of 45° at the 0.7R station. At the 0.7R
station the design lift coefficient of this blade was 0.3, the ratio
of blade-section chord to diameter was 0.066, and the maximum thick-
ness ratio was 0.08. Both the shrouded and unshrouded propellers
incorporated the NACA 16-series high-critical-speed airfoil sections
(reference 4).

The model shrouded propeller was 48 inches in diameter and the
clearance between the propeller tips and the shroud was approximately
$\frac{1}{16}$ inch. Although the model unshrouded propeller blades were
originally designed as a 48-inch diameter, it was necessary to test
them as a 49-inch-diameter propeller because a large hub size was
necessary to accommodate seven blades. The distance between propeller
center lines was kept as small as possible. This distance was
$4\frac{5}{8}$ inches for the shrouded propeller and $5\frac{1}{8}$ inches for the unshrouded.
The shrouded propeller was tested with spinners, while the unshrouded
propeller was tested without spinners. However, a check run made
with spinners on the unshrouded propeller indicated that the spinners
had a negligible effect.

TESTS

At a given rotational speed, readings were taken of the thrust
and torque of each component of the dual-rotating propellers and,
in the case of the shrouded propeller, a strain-gage reading was
taken and the multiple-tube manometer was photographed. These
readings were made at several values of propeller rotational speed
up to a maximum and in some cases repeated while decreasing the
rotational speed.

The tests were made with the front and rear propellers set at
equal blade angles. The unshrouded propeller tests covered a blade-
angle range from 15° to 40° in 5° increments, the blade angle being
measured at the 0.75R station. The shrouded propeller tests were

made at blade settings of 35°, 40°, and 45° except for the long shroud which was tested only at 40° blade angle.

As a check on the axial velocity distribution within the shroud, a run was made with a rake of total pressure and static tubes placed ahead of the propellers and then placed behind the propellers. This was done for the short cruise shroud with the front and rear propellers set at a blade angle of 40°.

The four dynamometer motors were driven by a single 1000-horsepower motor-generator set. Since the power absorbed by the two components of the dual-rotating propellers was not equal, there was a small difference in their rotational speed equal to the difference in slip of the front and rear motors. In the worst case this difference amounted to 4.8 percent of the front propeller rotational speed.

Tests were run only when the wind velocity was less than 6 miles per hour. This velocity was determined by a vane-type anemometer.

Calibrations of the dynamometer indicated that some friction was present in the system. This, coupled with the effect of wind, makes the data less accurate than those usually obtained in wind-tunnel propeller tests. However, the accuracy is sufficient for the purpose of comparing the shrouded and unshrouded propellers at static conditions. Figure 7 shows typical test results for the shrouded propeller.

REDUCTION OF DATA

The data have been reduced to thrust and power coefficients for each component of the dual-rotating propellers. The reduction of the data has been performed, as far as possible, to apply to the case of a propeller with both components operating at equal rotational speeds, that is, the coefficients of the front and rear components have been based on the rotational speed of the front and rear components, respectively. The tip Mach numbers of the front and rear components have been based only on the rotational speed of their respective components.

The measured static pressures on the shroud were reduced to a pressure coefficient C_p based on the rotational speed of the front propeller. A typical shroud pressure distribution is shown in figure 8 plotted against percent chord. The shroud thrust coefficient C_{T_S} was determined by the equation

$$C_{T_S} = \frac{T_S}{\rho n_F^2 D^4} = \frac{\pi}{2} \int C_p x \, dx$$

This thrust coefficient, then, was based on the rotational speed of the front propeller component.

RESULTS AND DISCUSSION

Action of shroud.— With the shrouded propeller running at static conditions, air is drawn into the front of the shroud from all directions. The typical shroud pressure distributions shown in figure 8 indicate that the air flows forward along the outside of the shroud and turns into the shroud, following the nose contour. It is evident that a low pressure and high velocity are reached at the nose which accounts for a large part of the shroud thrust. The shroud thereby assumes part of the propeller thrust so that the force in the propeller shaft is not a true measure of the thrust of the unit. The total thrust is then the sum of the propeller shaft thrust and shroud thrust.

At low propeller rotational speeds the flow separates from the shroud at the leading edge. Operation in this condition is rough and accompanied by much noise. As the propeller speed is increased, the flow suddenly becomes unseparated at the nose, resulting in smooth, quiet operation and much higher shroud thrust. This occurs at tip Mach numbers from 0.3 to 0.45, depending on the blade angle and shroud configuration. Comparison of shroud pressure distributions for the unseparated flow and separated flow conditions shows that they differ only in that the low-pressure region at the nose is lost in the separated flow condition. The shroud thrust in the separated flow condition is then only about half that obtained with the flow not separated from the shroud.

Results and comparison of propellers.— The basic data for the unshrouded propeller are shown in figures 9 and 10, while those for the shrouded propeller are shown in figures 11 to 16. The coefficients for the front and rear propellers are shown plotted against their respective tip Mach numbers. No data are presented for the shroud with flow separated. The results show that, with increasing blade angle, the front component of the unshrouded propeller stalls earlier than the rear component.

The shroud thrust presented in the figures was obtained from pressure measurements. This thrust represents an upper limit which probably could not be attained in practice for it does not include skin-friction drag and support-strut drag and interference. Check

points taken with the strain gages indicated a shroud thrust about
10 percent lower than the pressure measurements.

The shrouded and unshrouded propellers can best be compared
on an equal power-coefficient basis. Figure 17 shows the ratio
of total thrust coefficient to total power coefficient plotted
against total power coefficient for the unshrouded propeller and
for the shrouded propeller with the three shrouds tested. In the
range tested, for equal power the shrouded propeller produced more
than twice as much static thrust as the unshrouded propeller
chiefly because the unshrouded propeller was stalled while the
shrouded propeller was unstalled. Some improvement in the unshrouded
propeller could be expected if the blade section design lift coef-
ficients were higher.

Variations of shroud length and ratio of shroud exit area to
area at the propeller plane had little effect on the static thrust
coefficient of the shrouded propeller for a constant power coef-
ficient. However, this result could not be expected to hold for
very short shrouds.

Increasing the ratio of shroud exit area to area at the
propeller plane tended to decrease slightly the power coefficient
at a given blade angle because the inflow velocity increased. The
effect was greatest at the highest blade angle tested but even at
this point the power coefficient decreased only about 10 percent.

As previously mentioned, the shrouded-propeller thrust coef-
ficient was about twice that of the unshrouded propeller for equal
power coefficients. However, a fixed-pitch shrouded propeller
and a fixed-pitch unshrouded propeller, selected for a particular
full-scale application would probably not be of the same diameter
nor would they operate at the same rotational speed and power
coefficient at static conditions. The increase in static thrust
which would be realized by the use of a shrouded propeller depends,
then, on the particular operating conditions involved.

Comparison with theory.- Based on the simple momentum theory,
which ignores slipstream rotation and blade profile losses, the
equation for static thrust of an unshrouded propeller can be derived
as follows:

The contraction of the jet is such that

$$V_2 = \frac{1}{2}V_4$$

The power absorbed by the propeller is converted into kinetic energy in the final jet so that

$$P = \frac{1}{2}mV_4^2 = \frac{1}{4}\rho S_2 V_4^3$$

$$V_4 = \left(\frac{4P}{\rho S_2}\right)^{\frac{1}{3}}$$

Since the thrust equals mass flow multiplied by change in velocity,

$$T = mV_4 = \frac{\rho}{2}S_2\left(\frac{4P}{\rho S_2}\right)^{\frac{2}{3}}$$

$$T = 1.26\left(\rho S_2\right)^{\frac{1}{3}}\left(P\right)^{\frac{2}{3}} \tag{1}$$

The corresponding equation for the shrouded propeller is derived as follows by assuming that

$$p_3 = p_4$$

then,

$$V_2 = V_4\left(\frac{S_3}{S_2}\right)$$

The power absorbed by the propeller is converted into kinetic energy in the final jet so that

$$P = \frac{1}{2}mV_4^2 = \frac{1}{2}\rho S_2 V_4^3\left(\frac{S_3}{S_2}\right)$$

$$V_4 = \left(\frac{2P}{\rho S_3}\right)^{\frac{1}{3}}$$

Since the thrust equals mass flow multiplied by change in velocity,

$$T = mV_4 = \rho S_3 \left(\frac{2P}{\rho S_3}\right)^{\frac{2}{3}}$$

$$T = 1.588 \left(\rho S_3\right)^{\frac{1}{3}} \left(P\right)^{\frac{2}{3}} \tag{2}$$

Dividing equation (2) by equation (1),

$$\frac{T \text{ shrouded}}{T \text{ unshrouded}} = 1.26 \left(\frac{S_3}{S_2}\right)^{\frac{1}{3}} \tag{3}$$

for equal operating condition.

Equation (3) indicates that the shrouded propeller can be made greatly superior to the unshrouded by the use of a large shroud exit area whose function is to increase the momentum for a given power. The ideal theoretical values of thrust have been computed by the above equations for the model unshrouded propeller and for the model shrouded propeller with the short take-off shroud and the short cruise shroud. The ideal thrust is shown in figures 18 to 20 plotted against horsepower and the experimental total thrust is also plotted for comparison. For the unshrouded propeller, the curves show that in the higher blade angle range the static thrust is far below the ideal value because most of the blade is stalled. The shrouded propeller, however, produces thrust very close to the ideal value because the higher velocity through the propeller disk permits the blades to remain unstalled. The thrust of the propeller with the take-off shroud does not approach its ideal value as closely as does the propeller with the cruise shroud. This is probably the result of the larger diffuser angle of the take-off shroud.

The velocities ahead and behind the propellers are shown in figures 21 and 22 for several values of the front-propeller rotational speed. The tube locations are shown in the figures and the two planes at which the velocities were measured are indicated in figure 5. The results show that ahead of the propeller a velocity gradient exists such that the velocities near the shroud are higher than those near the nacelle. Measurements could not be made immediately ahead of the propeller but at this station the velocity distribution is probably much more uniform than at the station investigated. This is substantiated by the uniformity of the distribution directly

behind the propeller. The measurements are only approximate
since the construction of the rake was rough and the tubes were
mounted in an axial direction.

CONCLUSIONS

Static tests of unshrouded and shrouded dual-rotating
propellers indicate the following conclusions:

1. In the range tested, for equal power the shrouded
propeller produced approximately twice as much static thrust
as the unshrouded propeller chiefly because the unshrouded
propeller was stalled while the shrouded propeller was unstalled.

2. In the range tested, variations of shroud length and
ratio of shroud exit area to area at the propeller plane had
little effect on the static thrust of the shrouded propeller.

Langley Memorial Aeronautical Laboratory
     National Advisory Committee for Aeronautics
          Langley Field, Va.,

REFERENCES

1. Krüger, W.: Windkanalmessungen und Rechnungen zum Problem
     der ummantelten Luftschraube. Forschungsbericht Nr. 1949,
     Deutsche Luftfahrtforschung (Göttingen), 1944.

2. Regenscheit, B.: Standschubmessungen an zwei ummantelten
     Luftschrauben. UM Nr. 681, Deutsche Luftfahrtforschung
     (Göttingen), 1942.

3. Glauert, H.: Airplane Propellers. Windmills and Fans.
     Vol. IV of Aerodynamic Theory, div. L, ch. XI, sec. 6,
     W. F. Durand, ed., Julius Springer (Berlin), 1935,
     pp. 338-341.

4. Stack, John: Tests of Airfoils Designed to Delay the
     Compressibility Burble. NACA Rep. No. 763, 1943.

— Outer surface
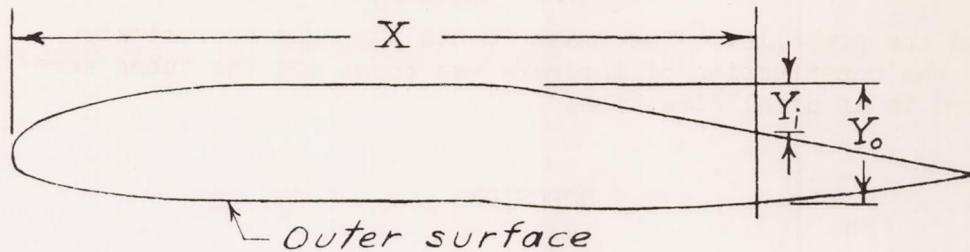
TABLE I.- SHROUD SECTION ORDINATES

[Stations and ordinates in percent of shroud chord]

| Shroud | | | | | | | | |
| Short, take-off | | | Long, take-off | | | Short, cruise | | |
X	Y_i	Y_o	X	Y_i	Y_o	X	Y_i	Y_o
0	7.52	7.52	0	6.03	6.03	0	7.52	7.52
.625	5.48	8.68	.625	4.24	7.05	.625	5.48	8.68
1.25	4.85	9.09	1.25	3.69	7.41	1.25	4.85	9.09
2.50	4.02	9.57	2.50	2.98	7.95	2.50	4.02	9.57
5.00	2.98	10.50	5.00	2.09	8.64	5.00	2.98	10.50
7.50	2.25	11.01	7.50	1.41	9.07	7.50	2.25	11.01
10.00	1.58	11.34	10.00	.86	9.30	10.00	1.58	11.34
15.00	.64	11.74	15.00	.21	9.57	15.00	.64	11.74
20.00	.19	11.97	20.00	.04	9.68	20.00	.19	11.97
25.00	.06	12.08	25.00	.00	9.70	25.00	.06	12.08
30.00	.02	12.08	30.00	.00	9.70	30.00	.02	12.08
40.00	.00	12.08	39.00	.00	9.70	40.00	.00	12.08
48.50	.00	12.08	40.00	.00	9.75	48.50	.00	12.08
50.00	.00	12.19	45.00	.42	10.00	50.00	.00	12.05
55.00	.68	12.49	50.00	1.04	10.17	55.00	.31	11.95
60.00	1.63	12.70	60.00	2.29	10.24	60.00	.62	11.58
70.00	3.60	12.71	70.00	3.54	9.92	70.00	1.24	10.17
80.00	5.57	12.12	80.00	4.79	9.40	80.00	1.86	8.22
90.00	7.54	11.09	90.00	6.04	8.59	90.00	2.48	5.81
100.00	9.52	9.67	100.00	7.30	7.48	100.00	3.10	3.26

NATIONAL ADVISORY
COMMITTEE FOR AERONAUTICS
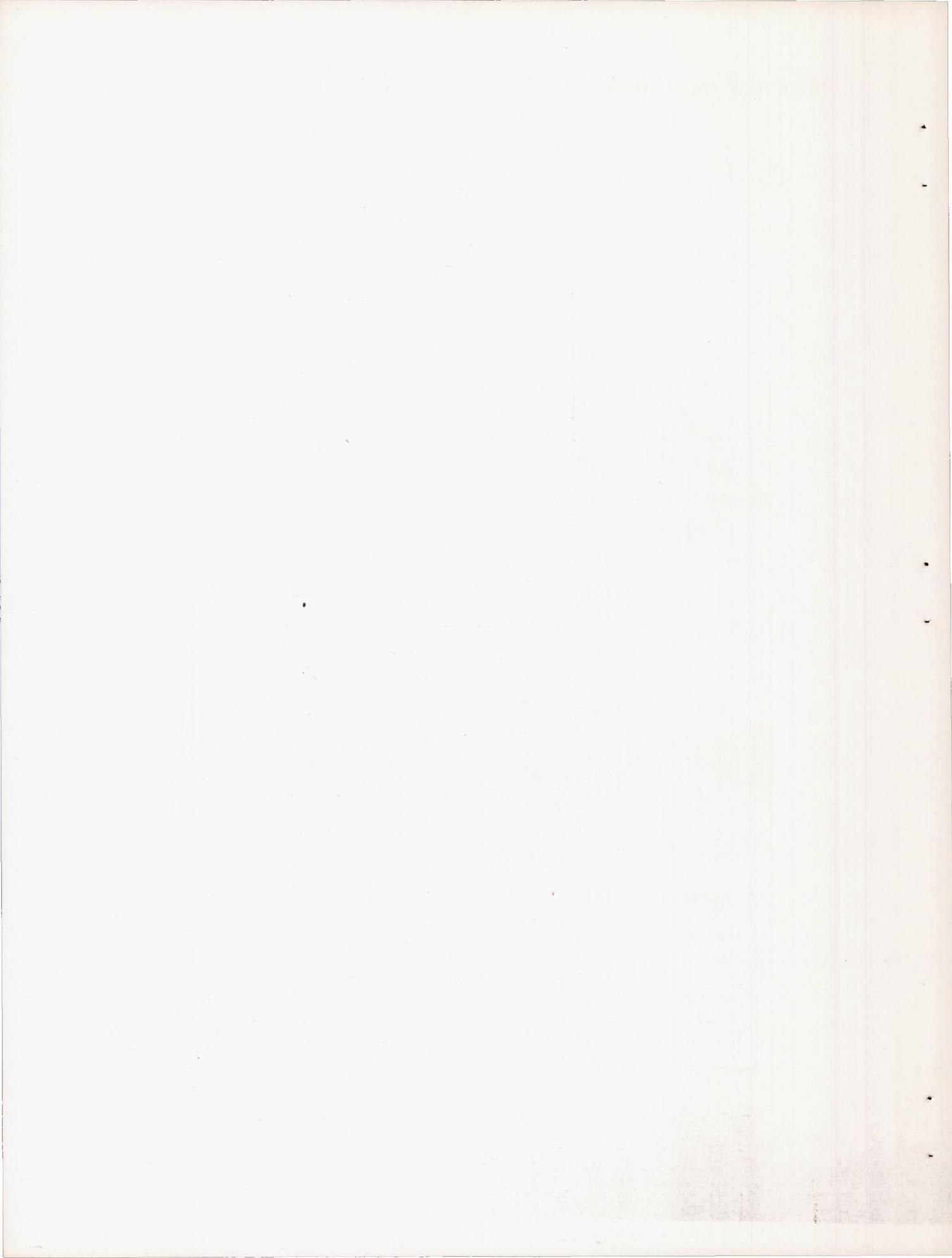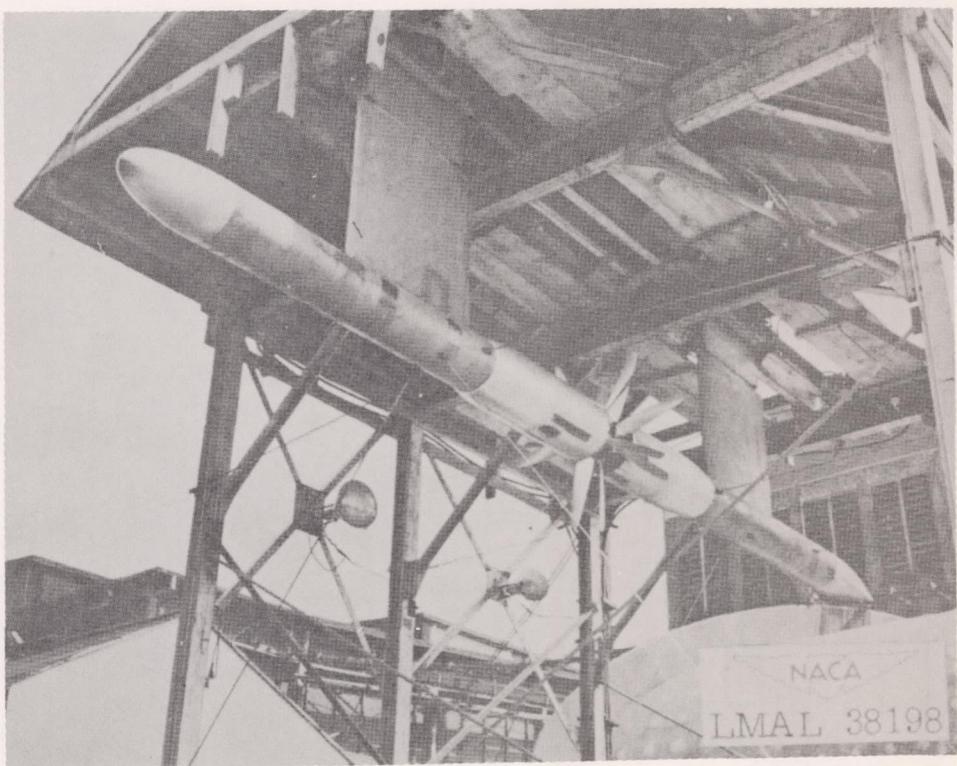
Figure 1.- Static test setup with unshrouded propeller.
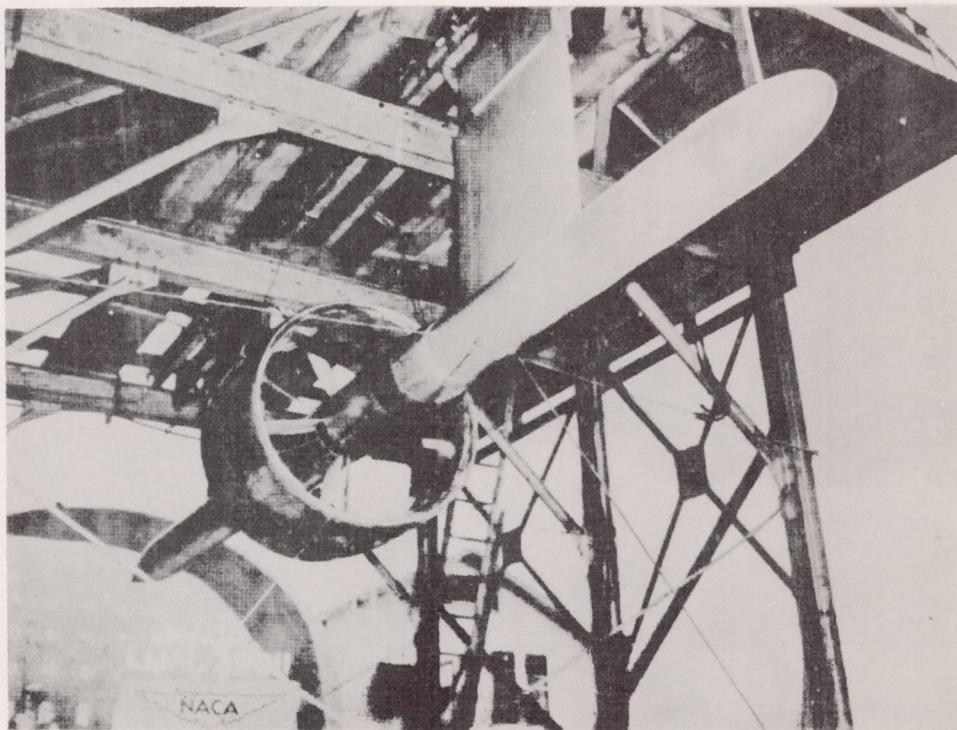
Figure 2.- Static test setup with shrouded propeller.
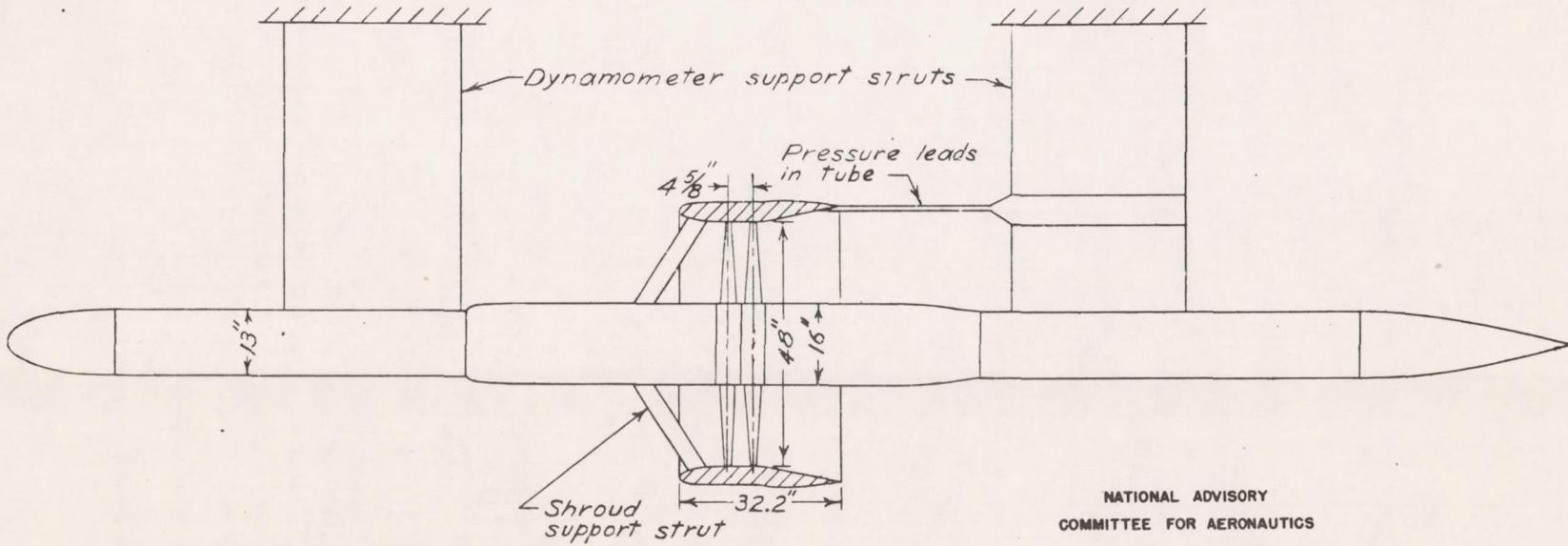
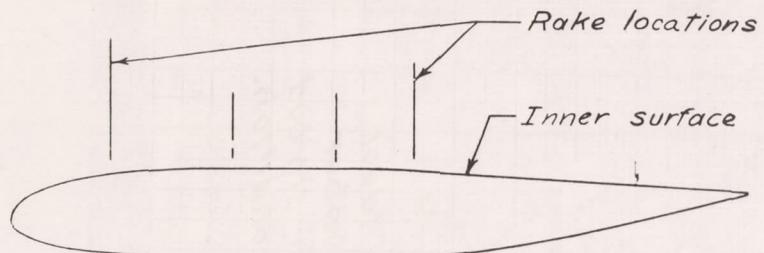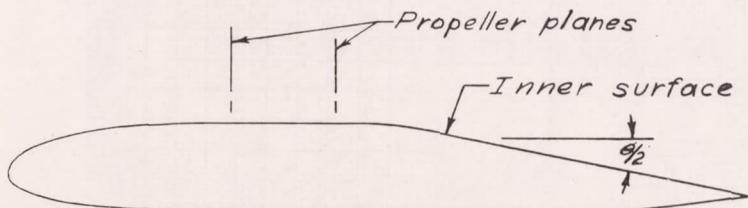Figure 3.— Side view of dynamometer with propeller and short, take-off shroud.

NATIONAL ADVISORY
COMMITTEE FOR AERONAUTICS
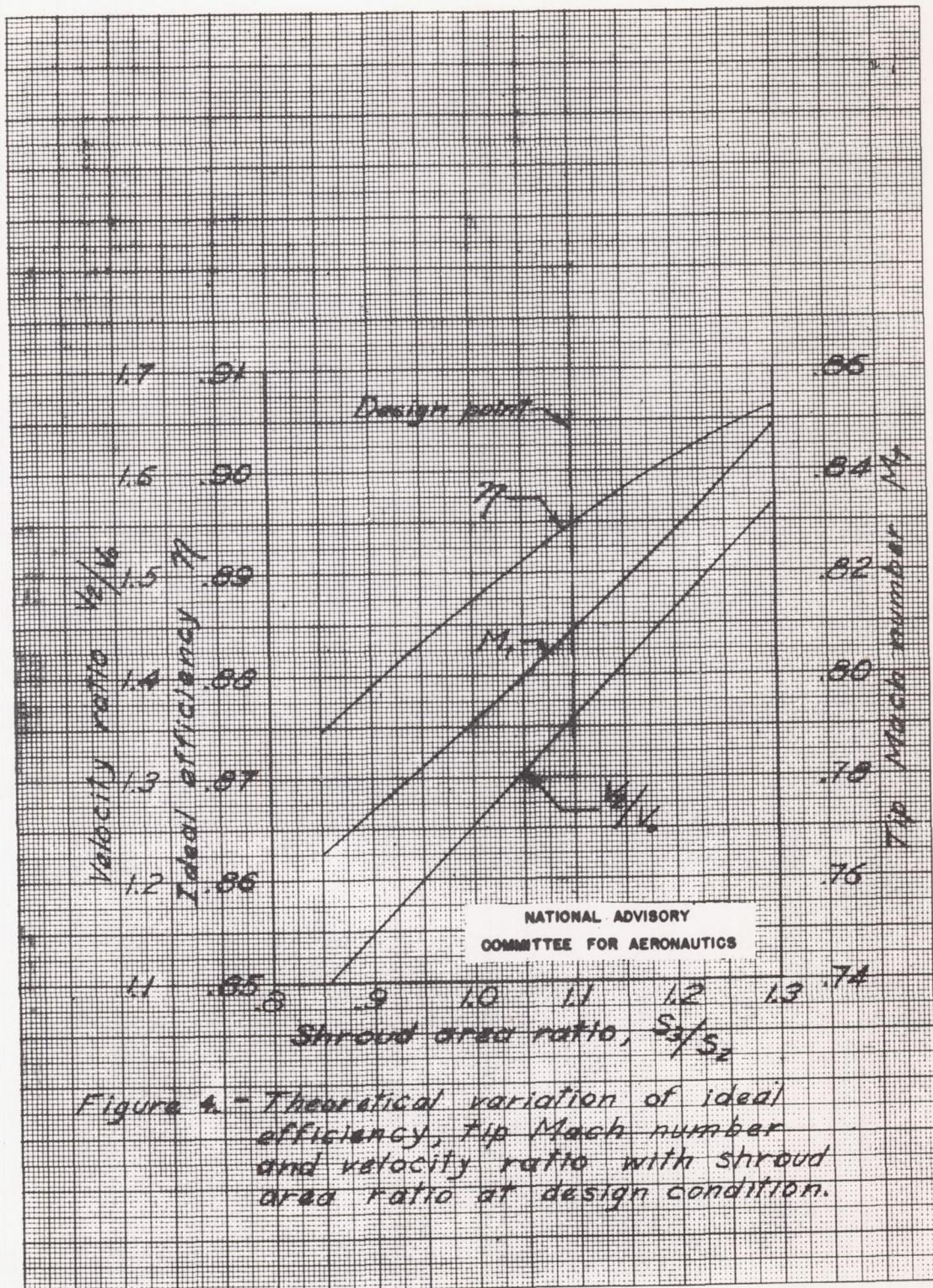
Figure 4. – Theoretical variation of ideal
efficiency, tip Mach number
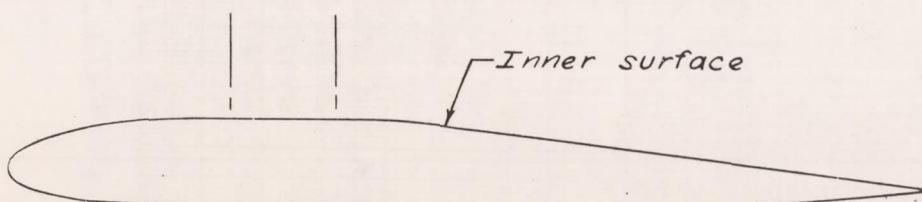and velocity ratio with shroud
area ratio at design condition.

Rake locations

Inner surface

(a) Short, cruise shroud

Propeller planes

Inner surface

$\theta/2$

(b) Short, take-off shroud

Inner surface

(c) Long, take-off shroud

l, inches	l/D	S_3/S_2	θ, degrees
32.2	0.671	1.1	7.0
32.2	0.671	1.3	22.4
40.1	0.836	1.3	14.4

NATIONAL ADVISORY
COMMITTEE FOR AERONAUTICS

Figure 5.- Shroud forms tested.
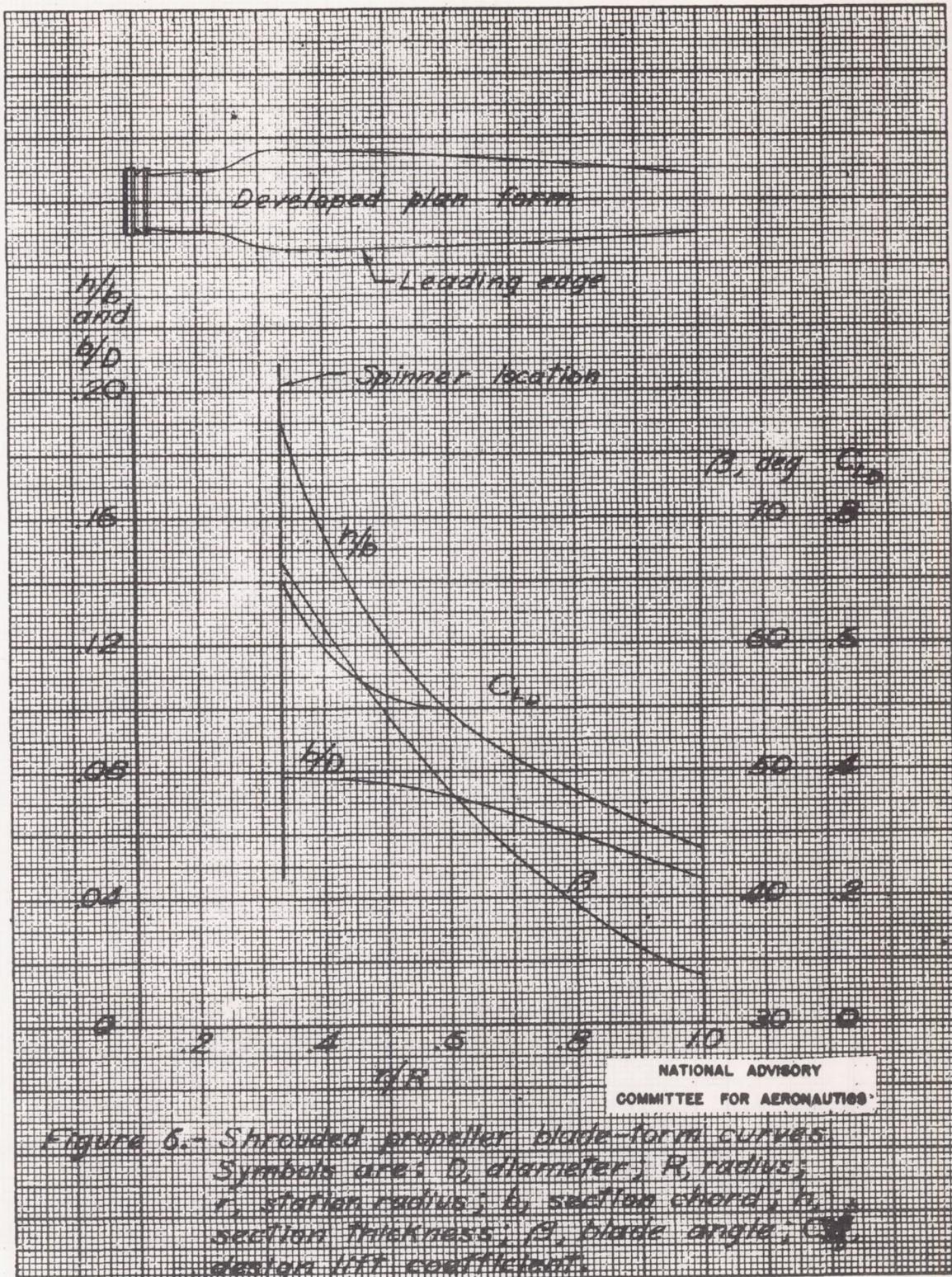
Figure 6.- Shrouded propeller blade-form curves. Symbols are: D, diameter; R, radius; r, station radius; b, section chord; h, section thickness; β, blade angle; C_{L_D}, design lift coefficient.

Figure 7.- Typical test results. Shrouded propeller with short, take-off shroud. $\beta_F = \beta_R = 40°$ (Flagged symbols denote decreasing rotational speed).

Figure 8.- Typical shroud pressure distribution. Short, take-off shroud.
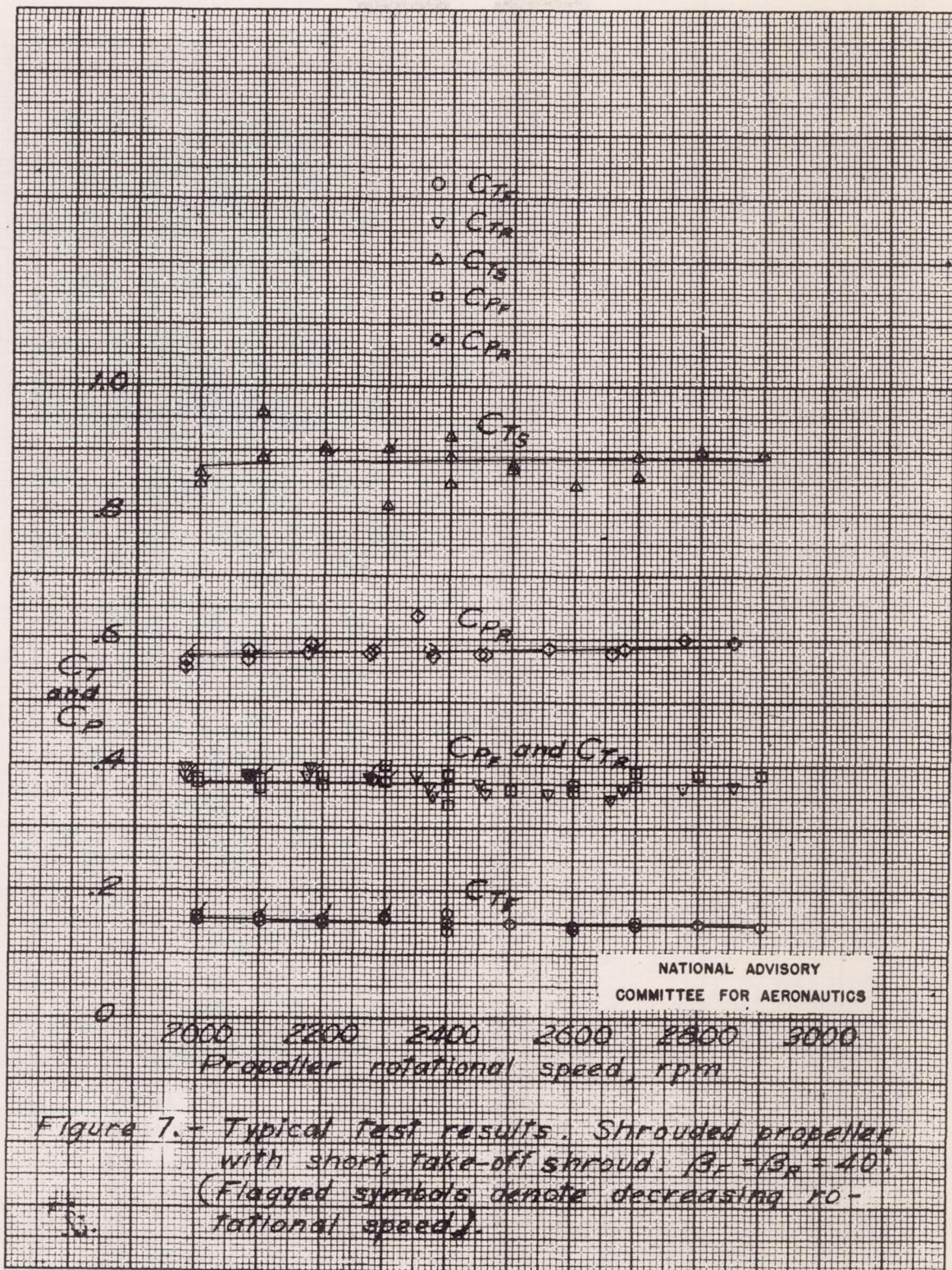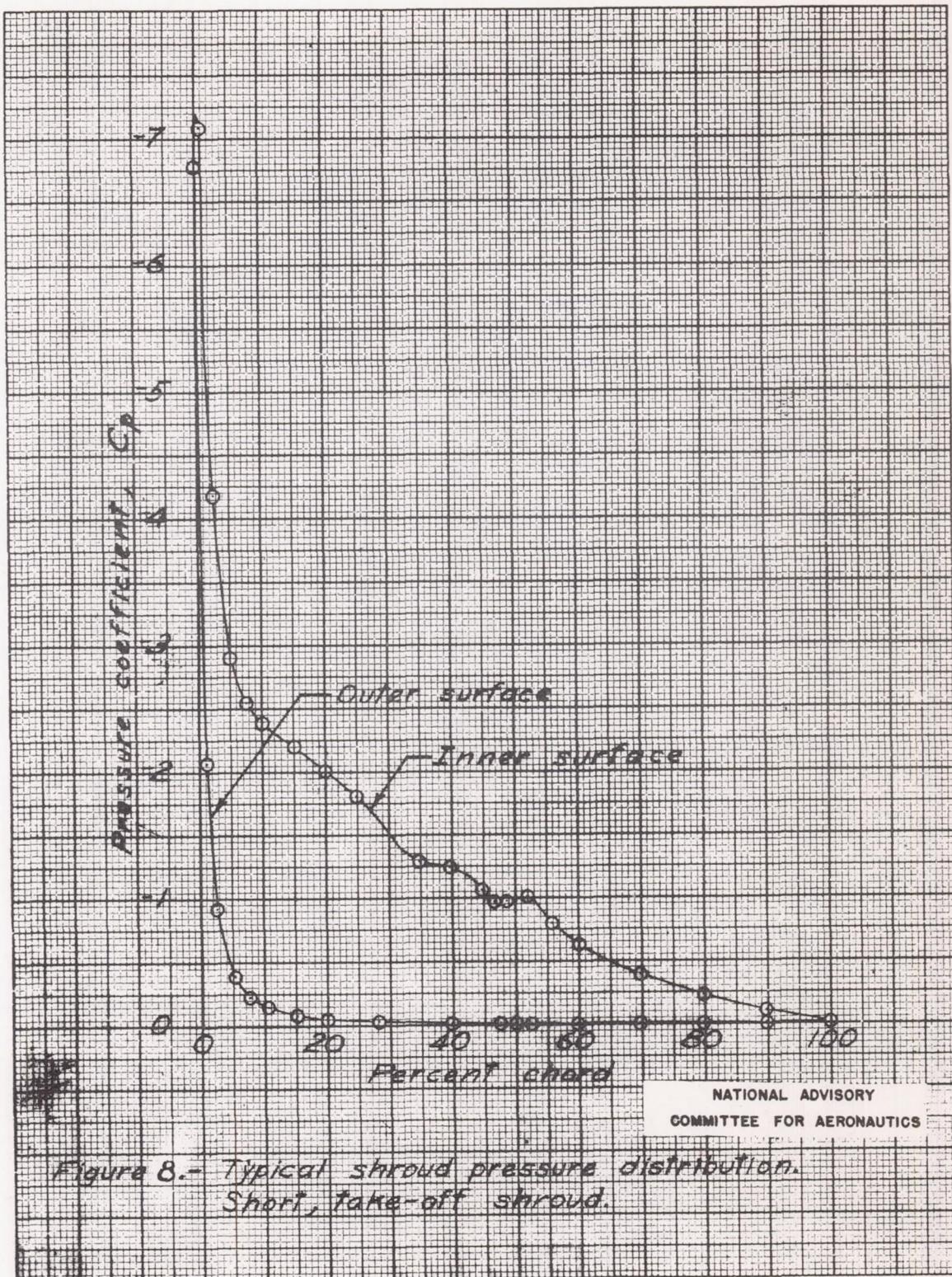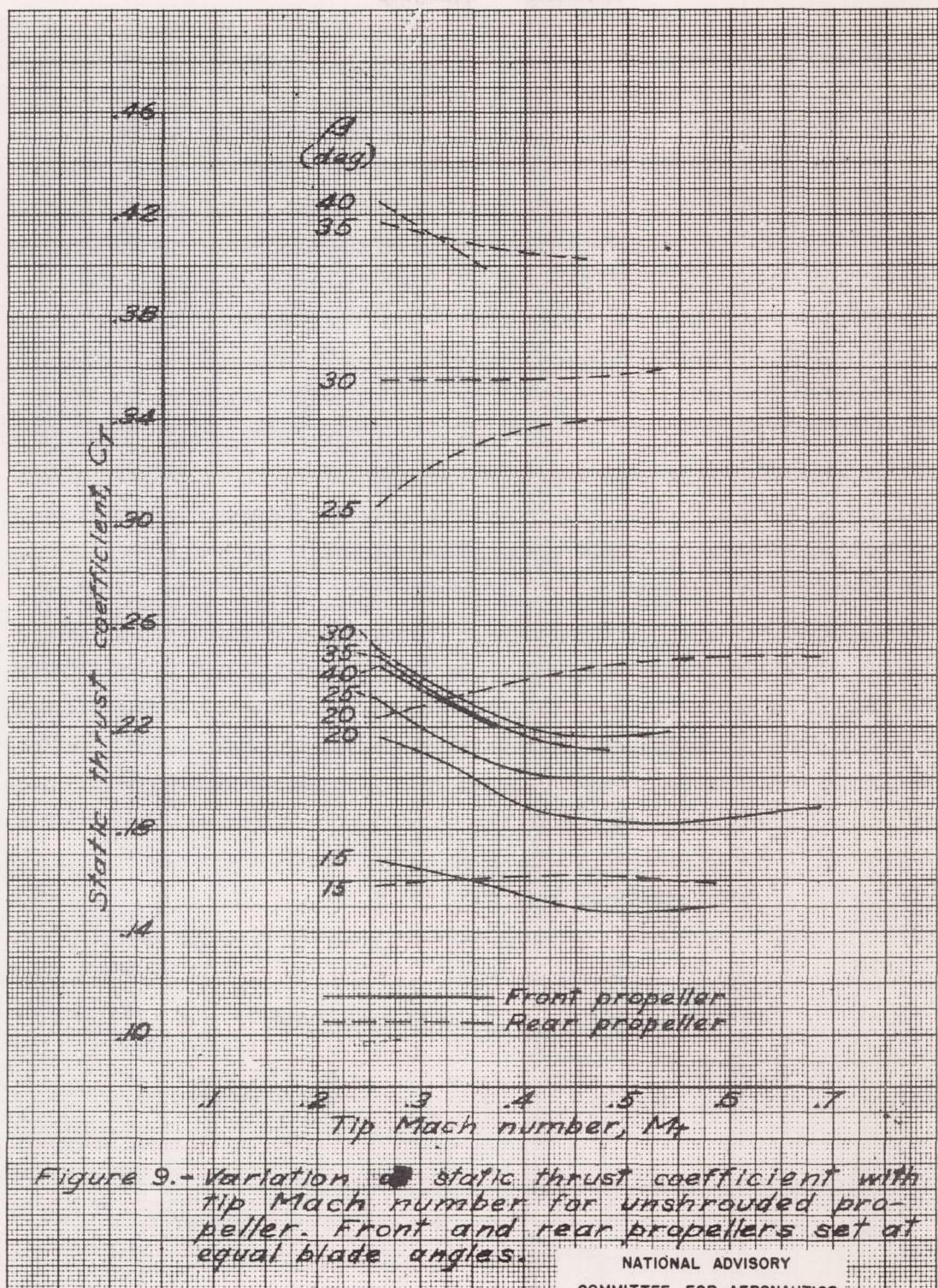
Figure 9.- Variation of static thrust coefficient with tip Mach number for unshrouded propeller. Front and rear propellers set at equal blade angles.
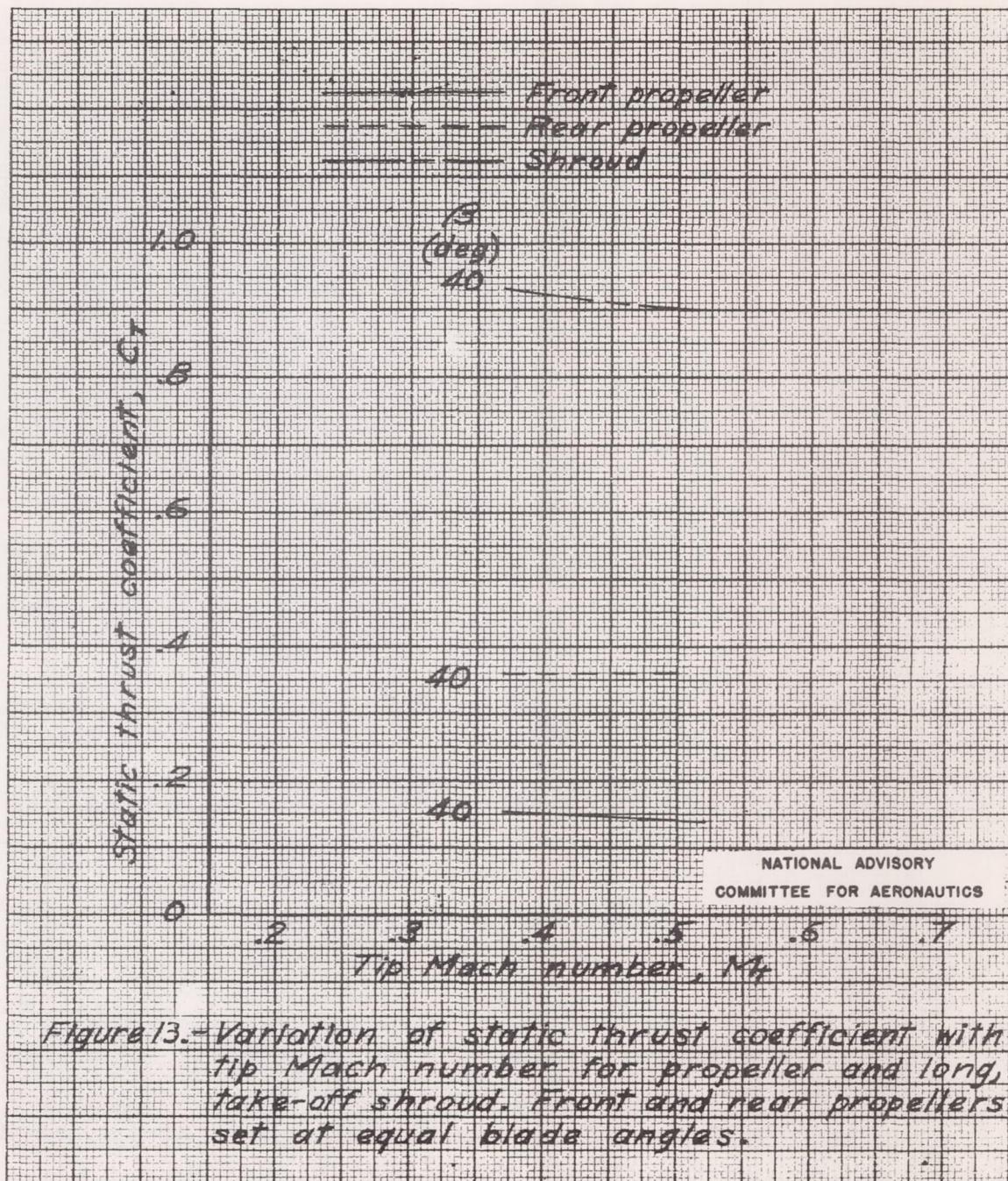
Figure 10.- Variation of static power coefficient with tip Mach number for unshrouded propeller. Front and rear propellers set at equal blade angles.
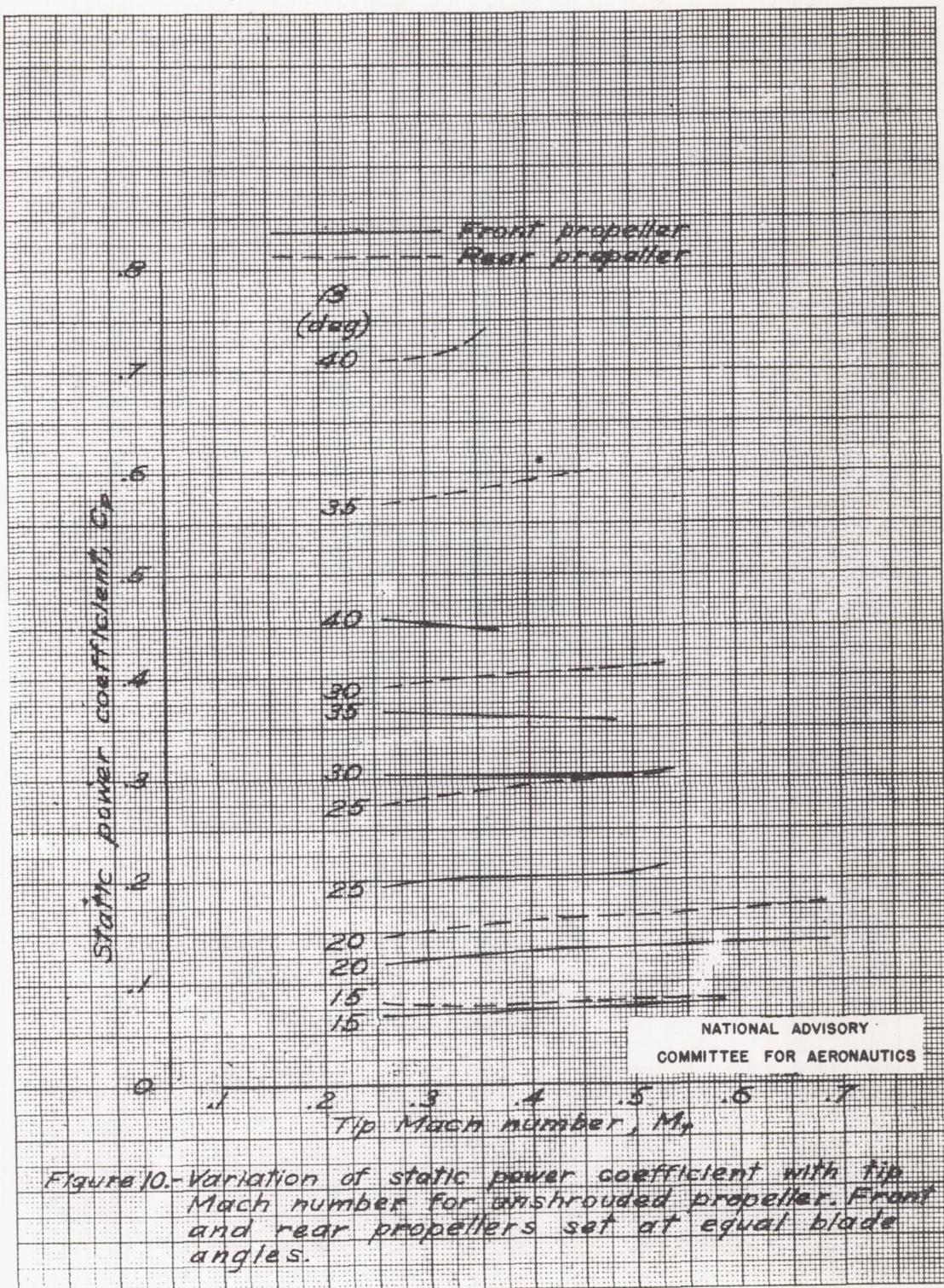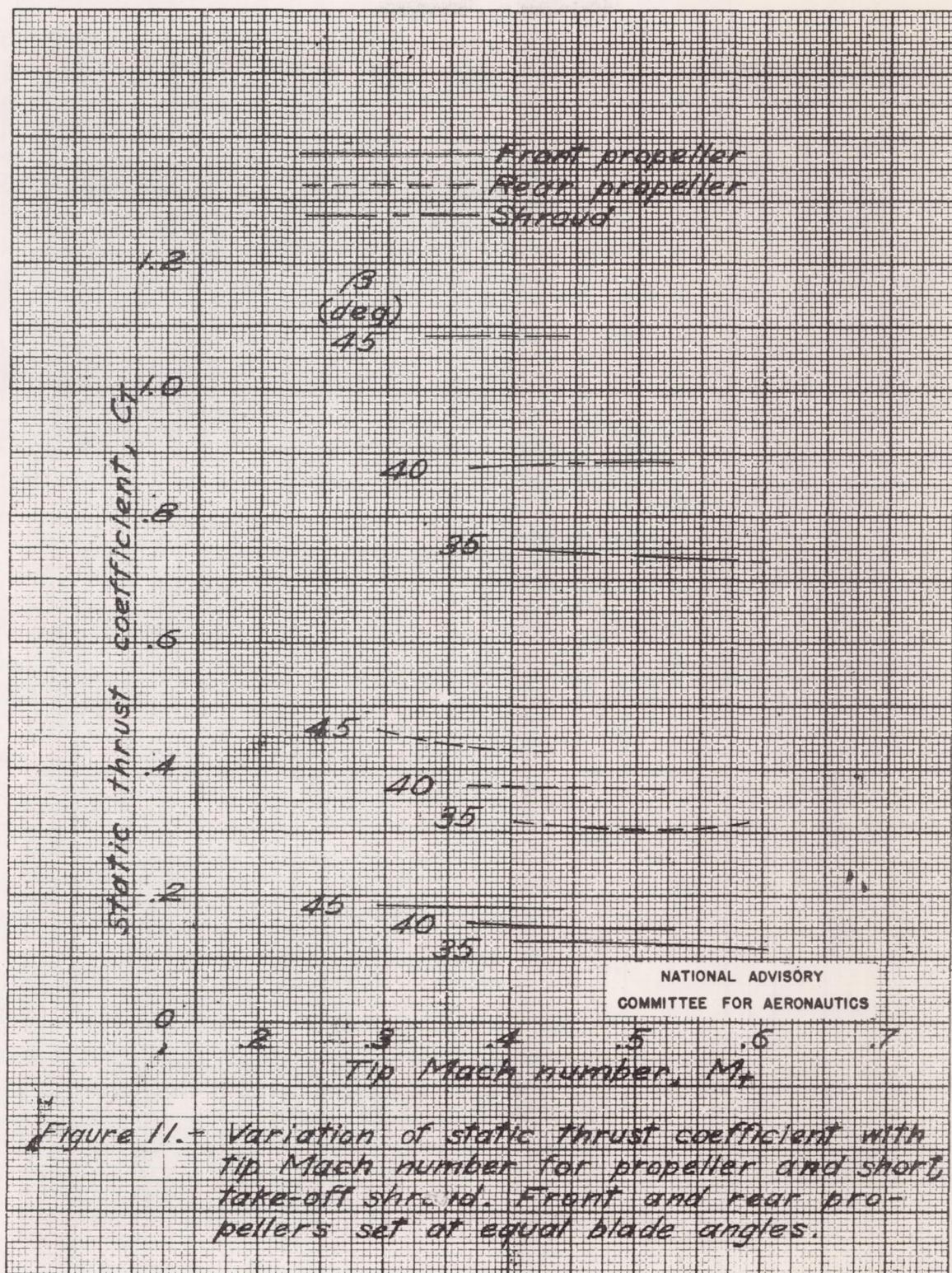
Figure 11.- Variation of static thrust coefficient with tip Mach number for propeller and short take-off shroud. Front and rear propellers set at equal blade angles.
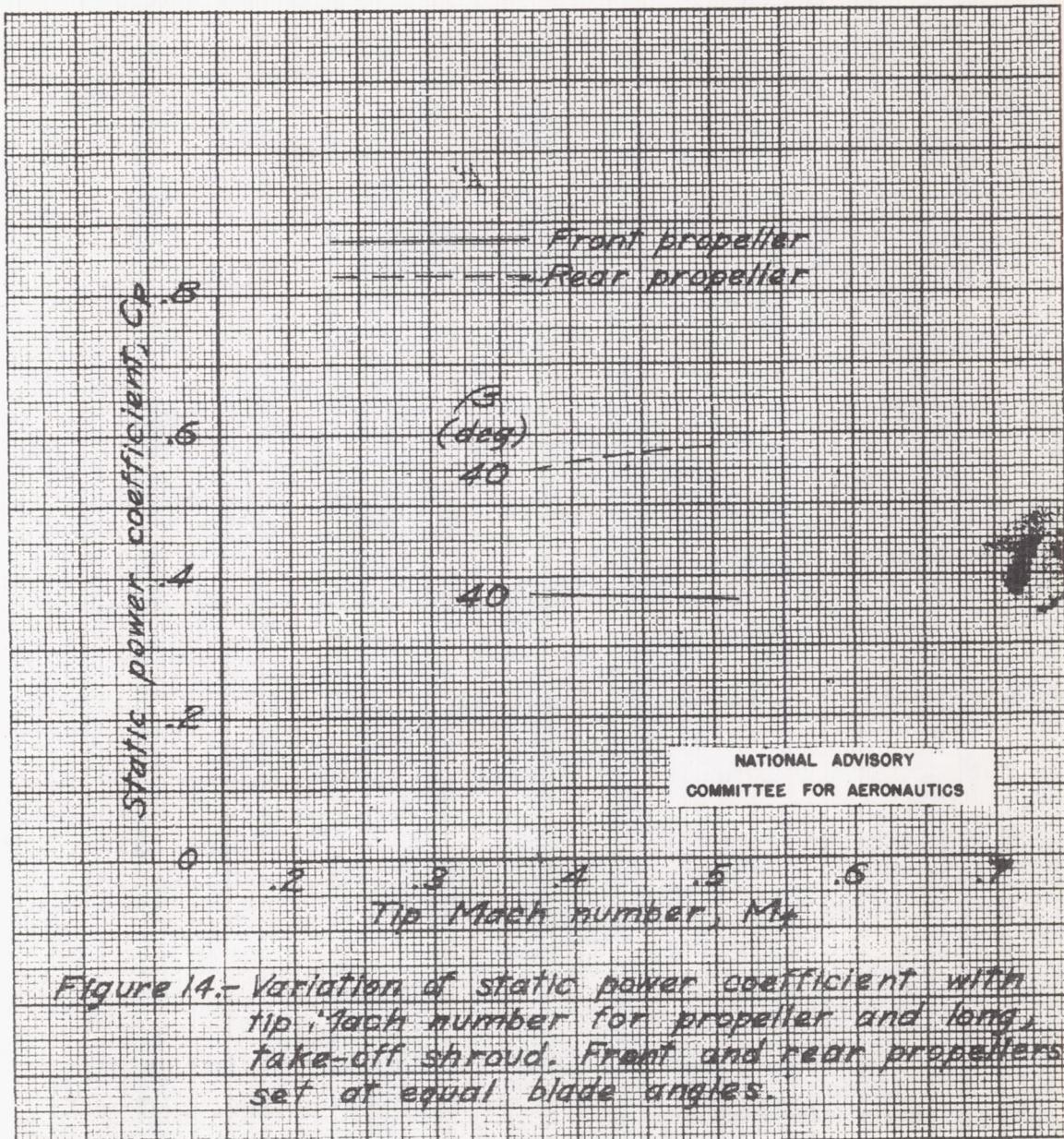
Figure 12.— Variation of static power coefficient with tip Mach number for propeller and short, take-off shroud. Front and rear propellers set at equal blade angles.
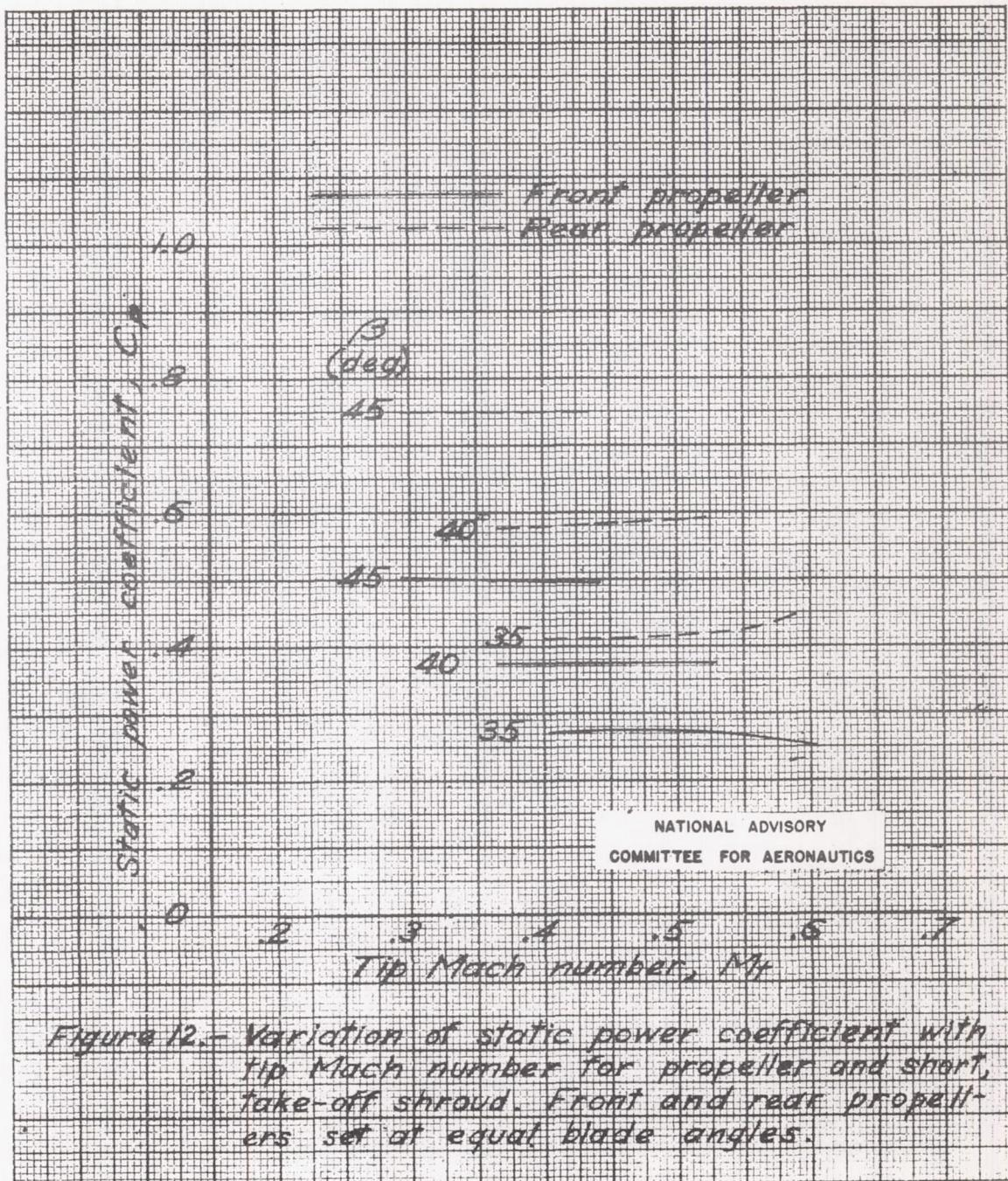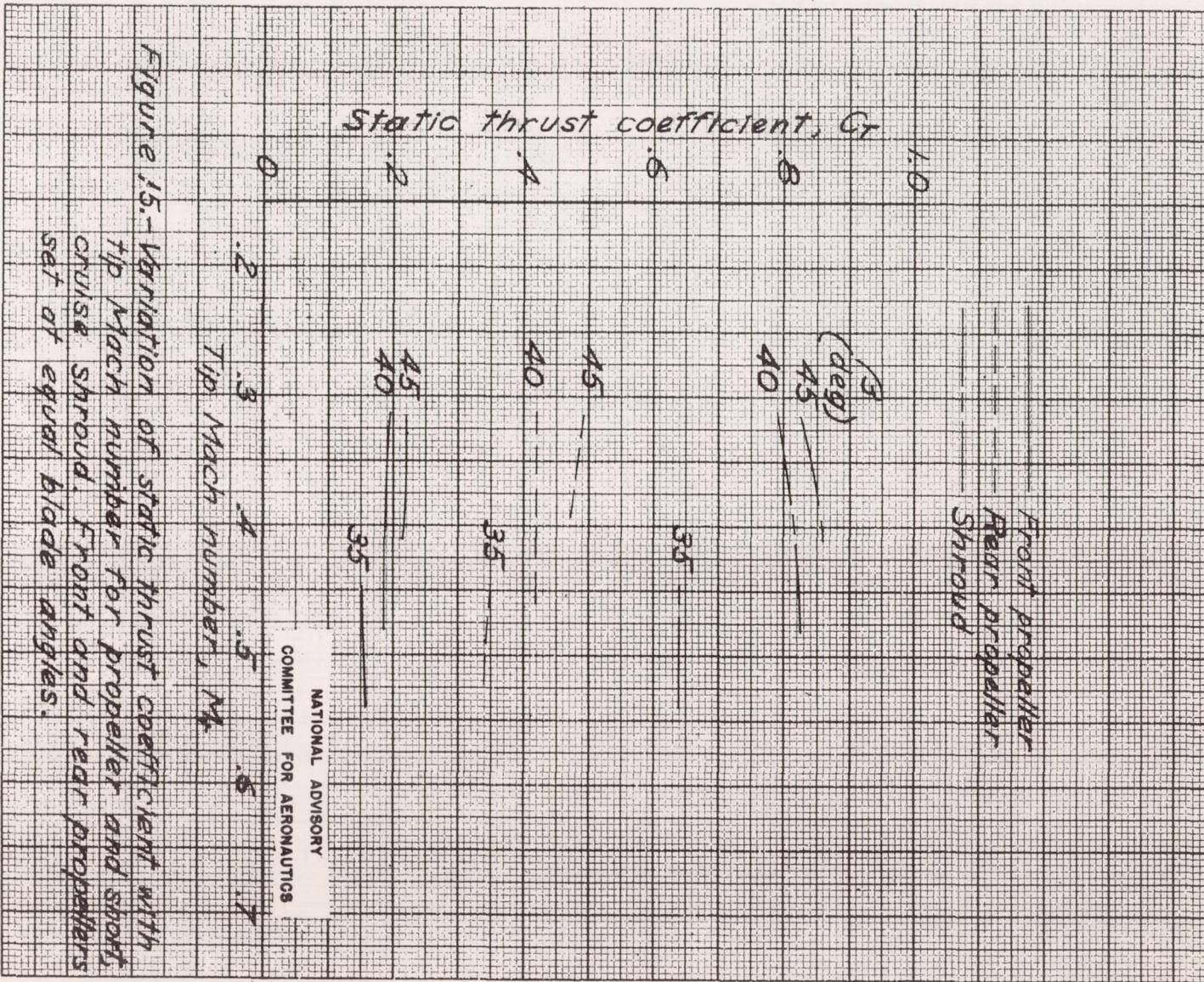
Figure 13.- Variation of static thrust coefficient with tip Mach number for propeller and long, take-off shroud. Front and rear propellers set at equal blade angles.
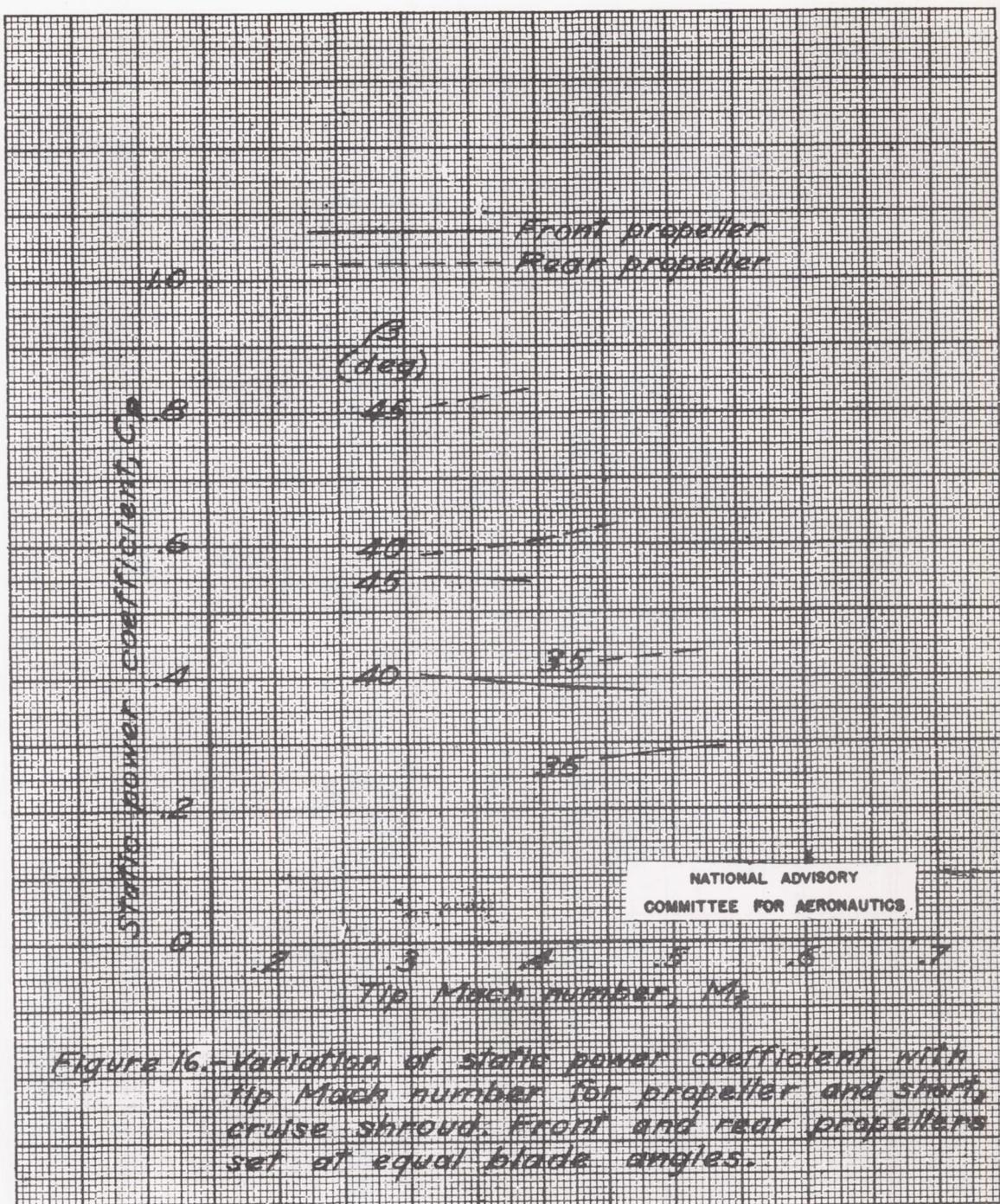
Figure 14.- Variation of static power coefficient with tip Mach number for propeller and long, take-off shroud. Front and rear propellers set at equal blade angles.

Static thrust coefficient, C_T

Front propeller
Rear propeller
Shroud

β
(deg)

Tip Mach number, M_t

NATIONAL ADVISORY
COMMITTEE FOR AERONAUTICS

Figure 15.- Variation of static thrust coefficient with tip Mach number for propeller and short cruise shroud. Front and rear propellers set at equal blade angles.
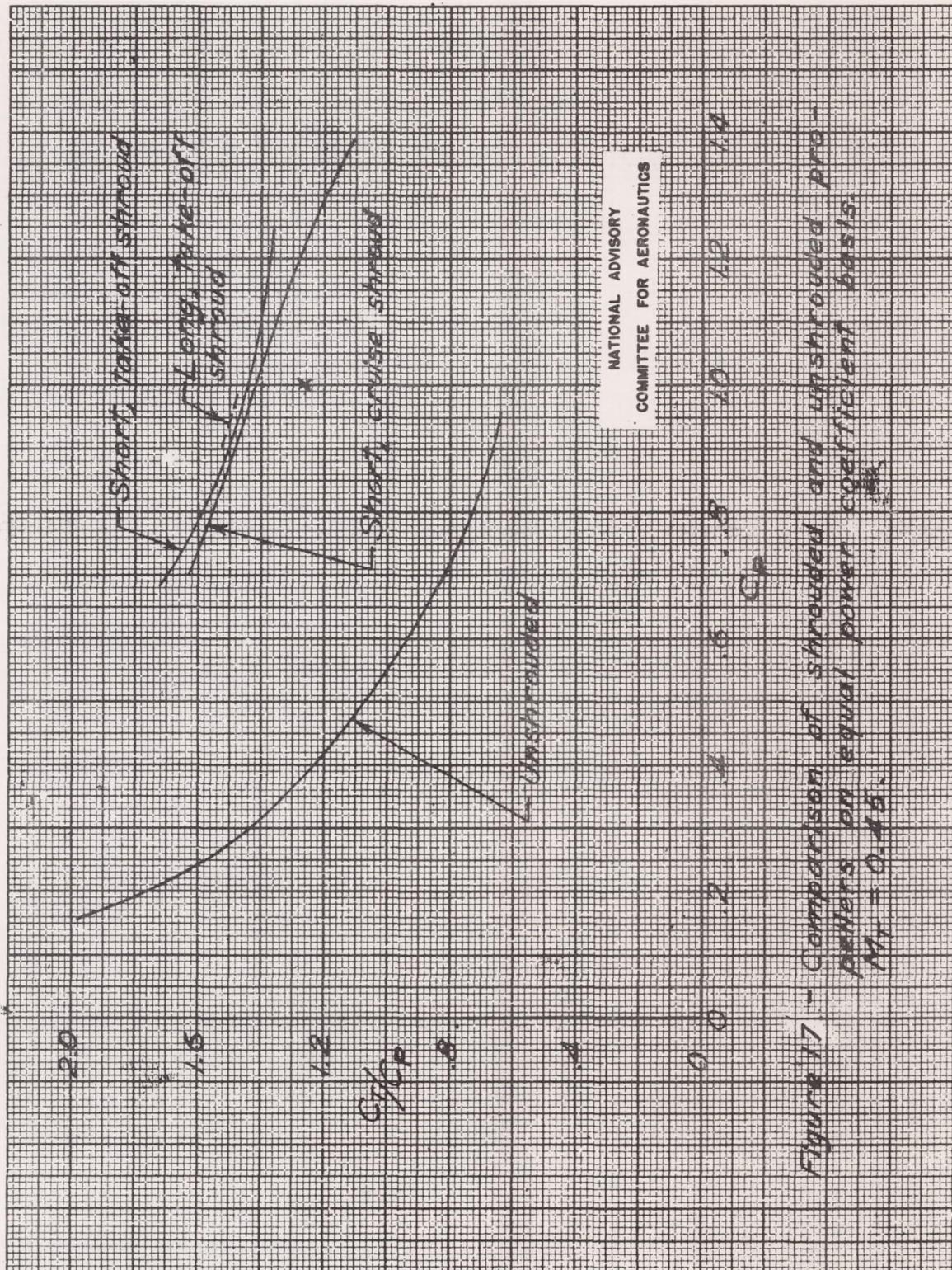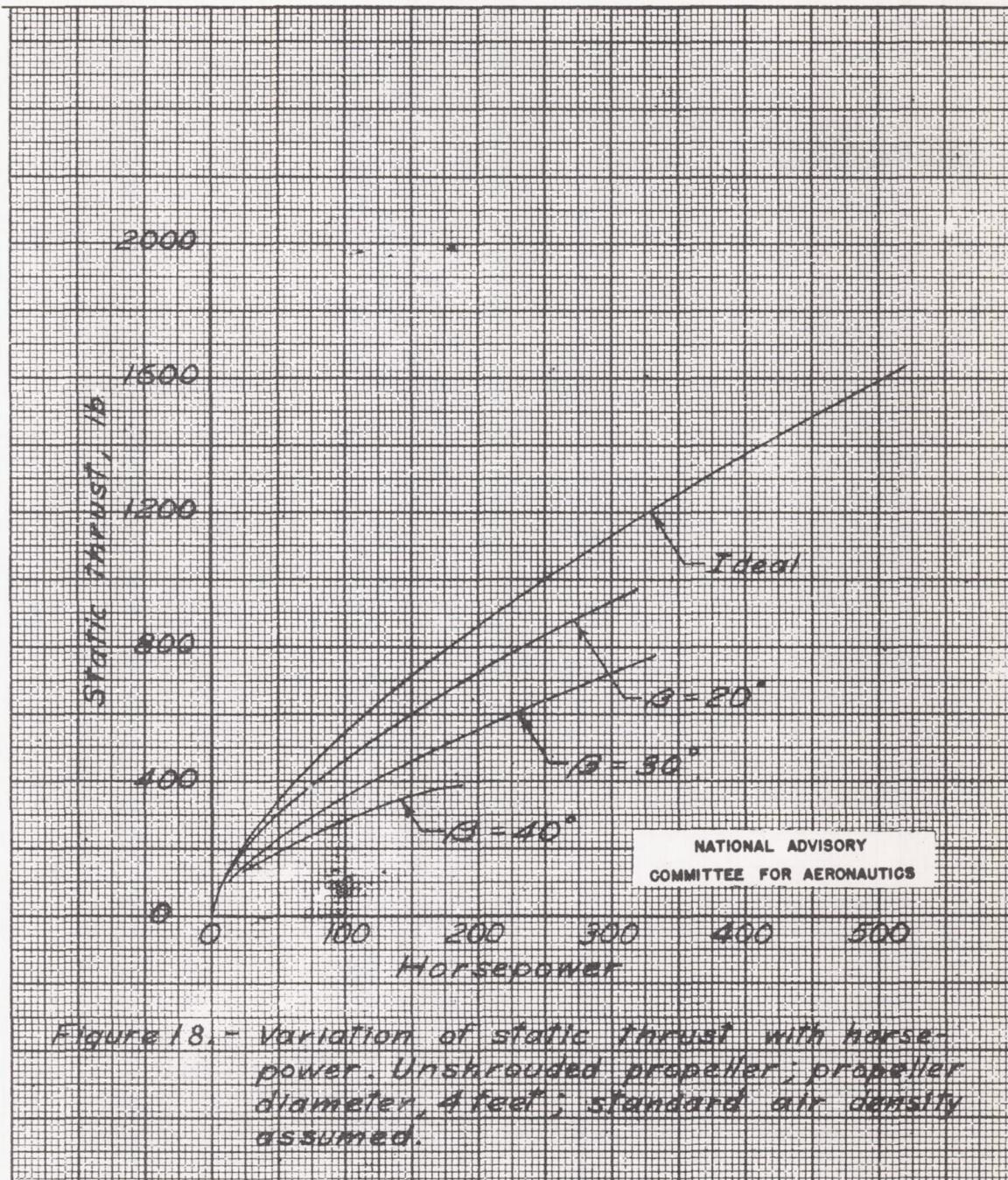
Figure 16.- Variation of static power coefficient with
tip Mach number for propeller and short
cruise shroud. Front and rear propellers
set at equal blade angles.

Figure 17.- Comparison of shrouded and unshrouded pro-
pellers on equal power coefficient basis.
$M_T = 0.45$.

Figure 18.- Variation of static thrust with horse-
power. Unshrouded propeller; propeller
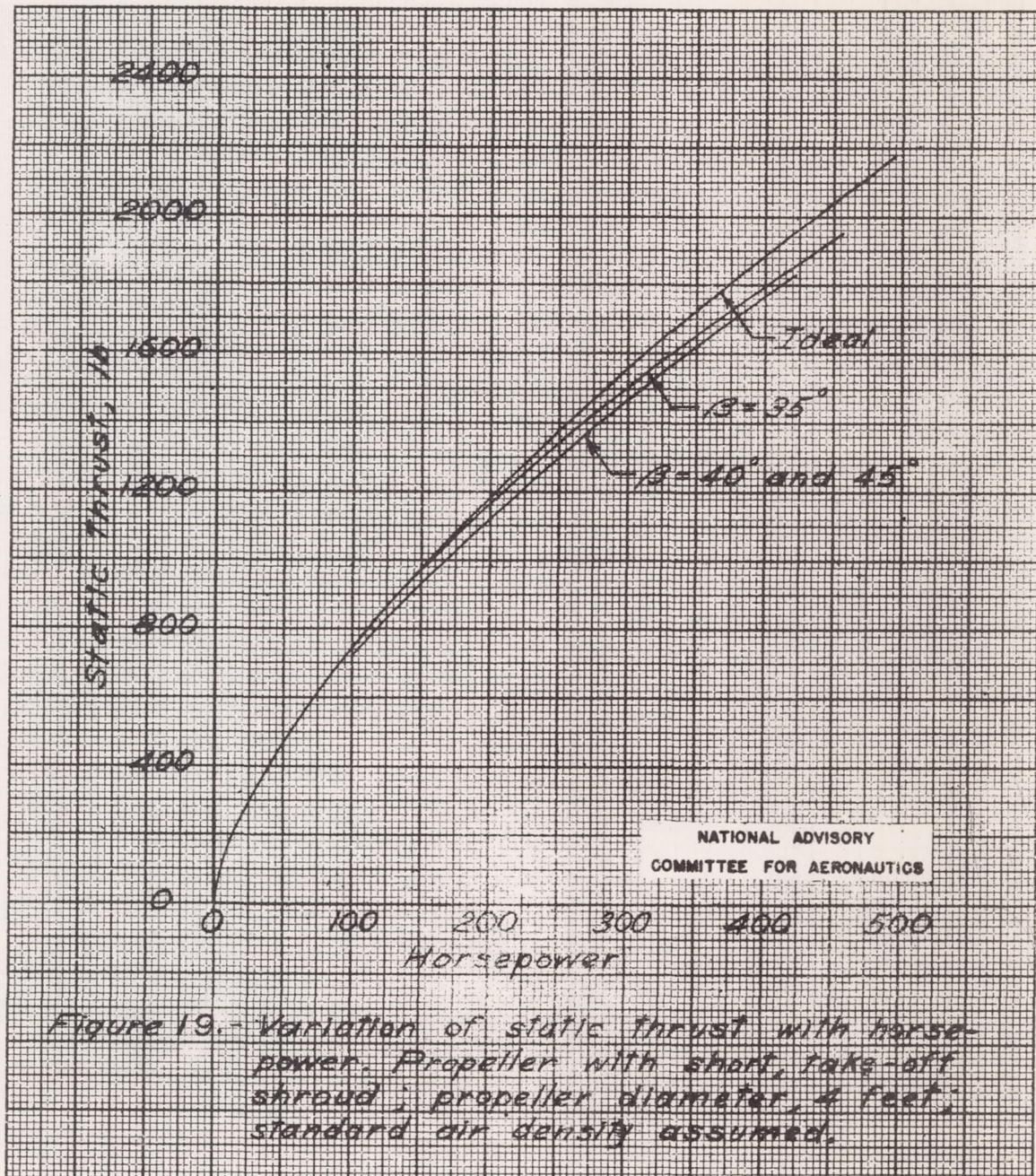diameter, 4 feet; standard air density
assumed.

Figure 19.- Variation of static thrust with horsepower. Propeller with short take-off shroud; propeller diameter, 4 feet; standard air density assumed.
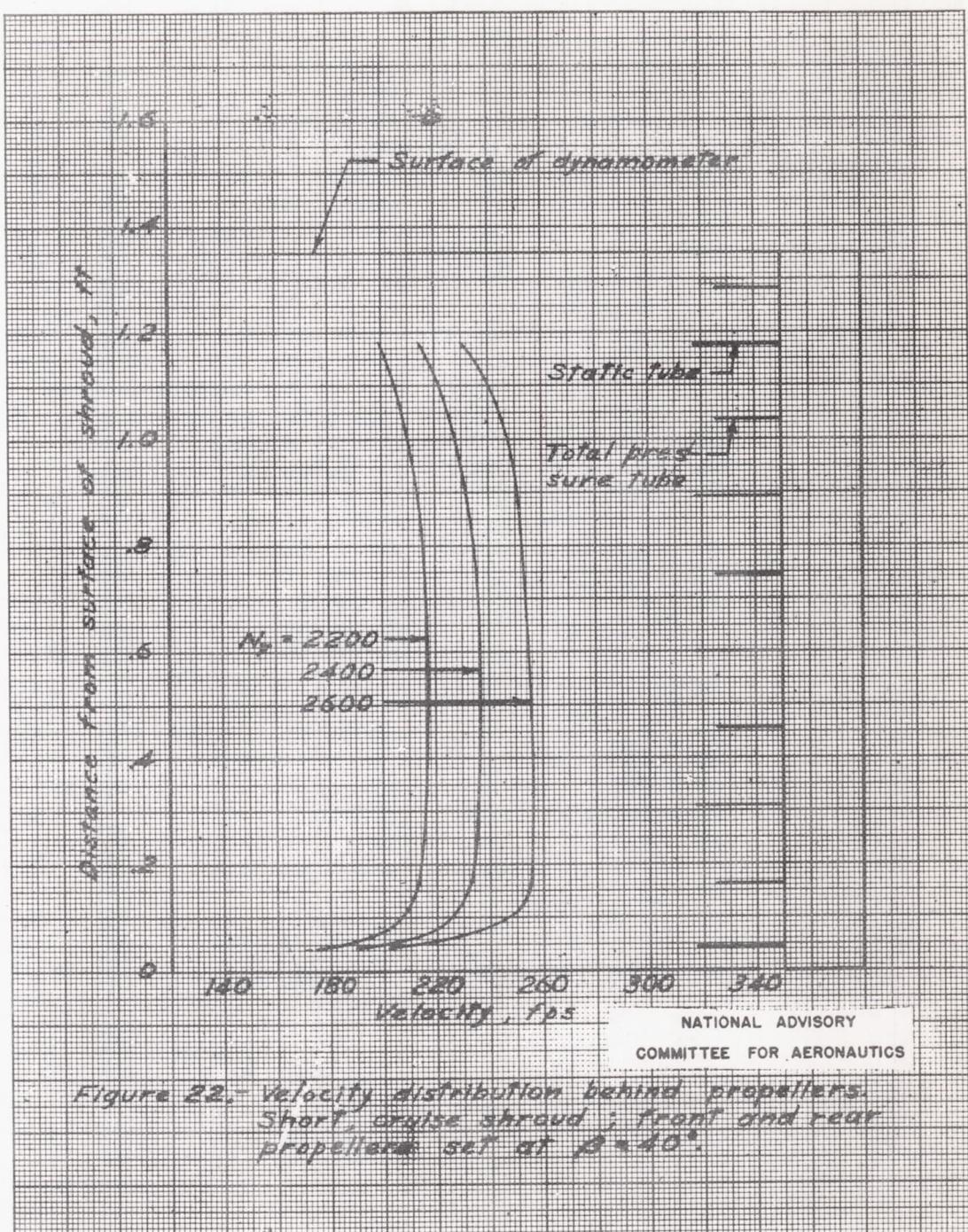
Figure 20.- Variation of static thrust with horse-
power. Propeller with short, cruise
shroud; propeller diameter, 4 feet;
standard air density assumed.

Figure 21.- Velocity distribution ahead of propellers. Short, cruise shroud; front and rear propellers set at β = 40°.
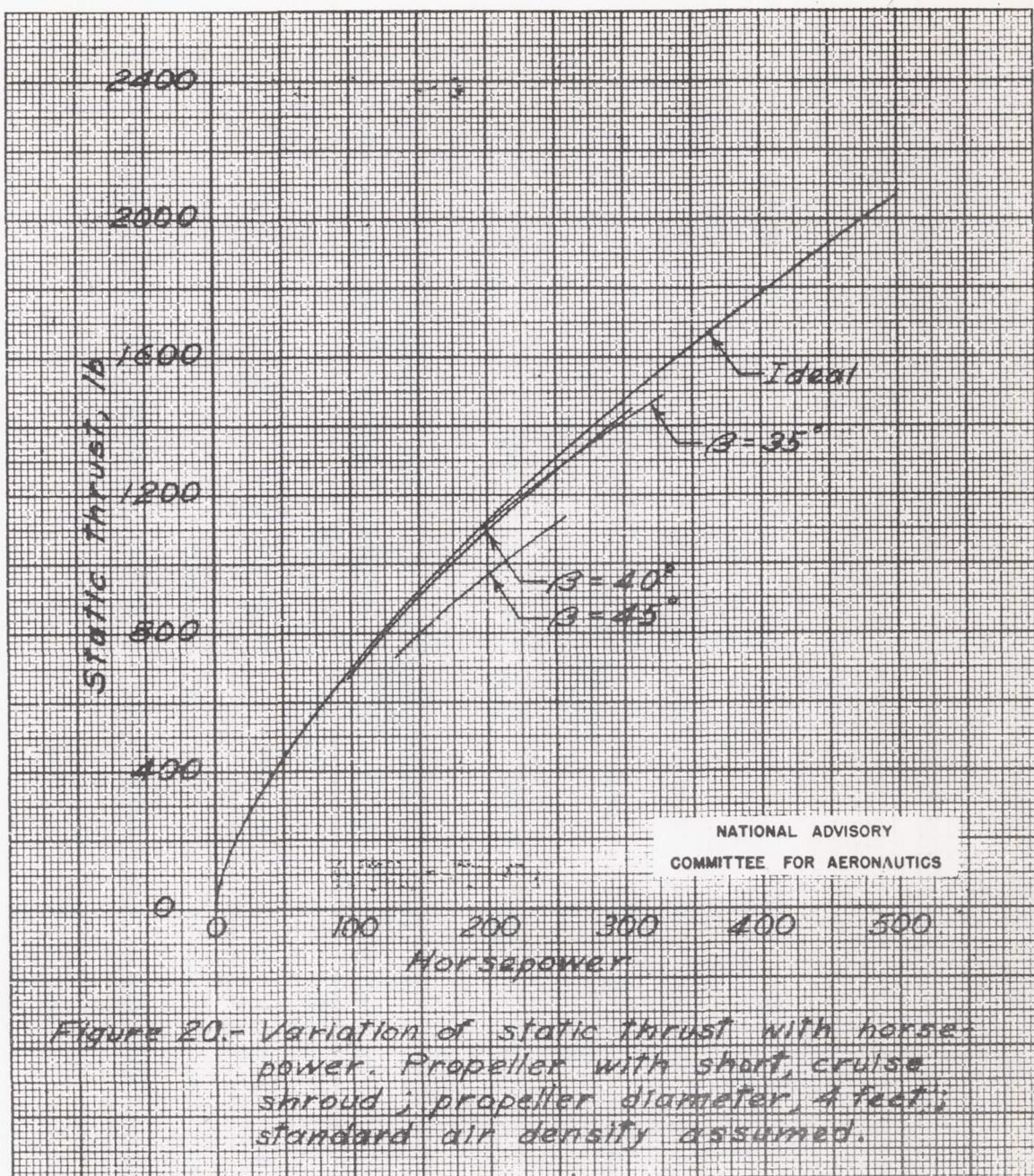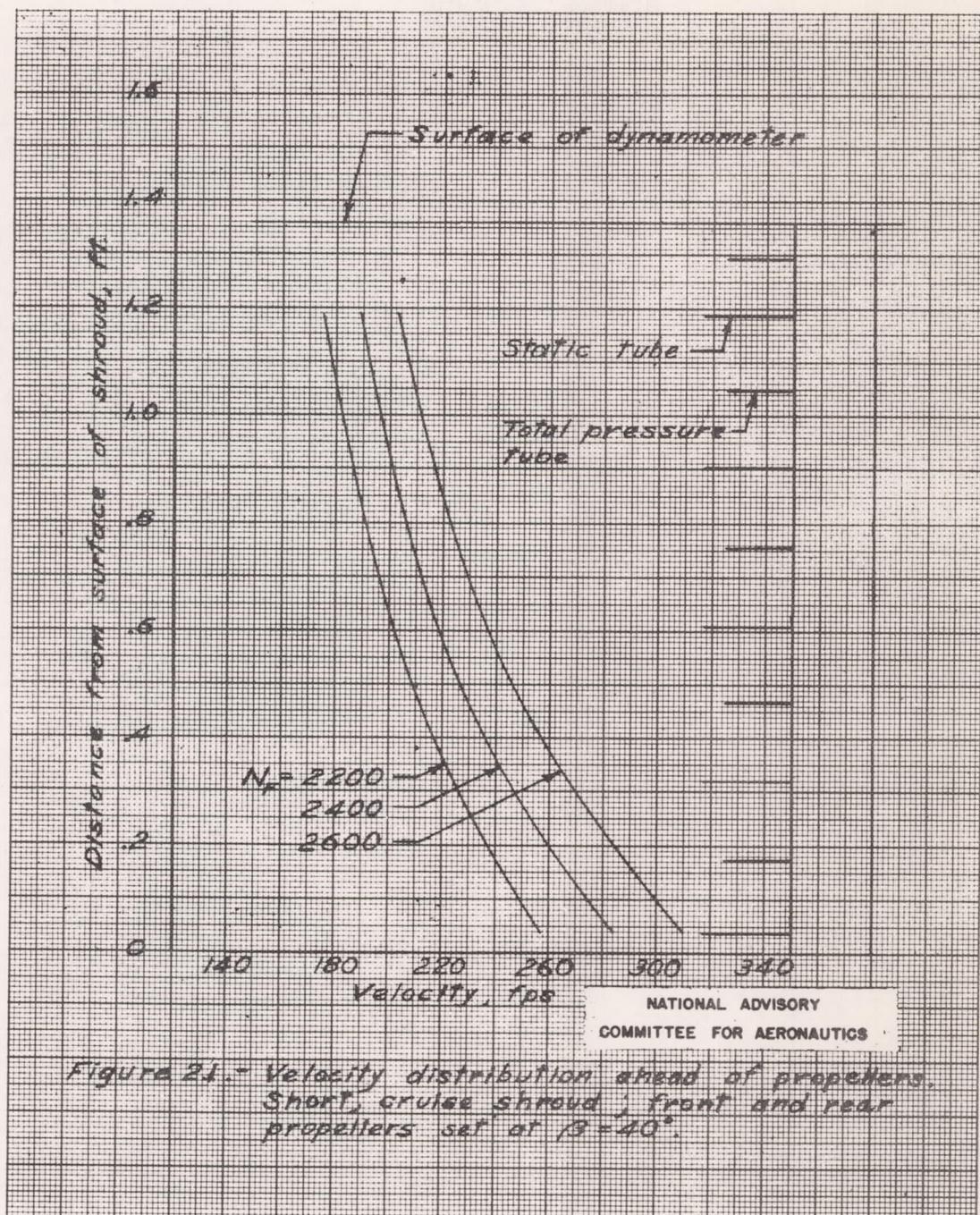
Figure 22. Velocity distribution behind propellers. Short, cruise shroud ; front and rear propellers set at β = 40°.